Parameter Estimation of Isotropic PMSMs Based on Multiple Steady-State Measurements Collected During Regular Operations

Parameter Estimation of Isotropic PMSMs Based on Multiple Steady-State Measurements Collected During Regular Operations

Elia Brescia, Paolo Roberto Massenio, Mauro Di Nardo, *IEEE Member*, Giuseppe Leonardo Cascella, *IEEE Member*, Chris Gerada, *IEEE Senior Member*, and Francesco Cupertino, *IEEE Senior Member*

***Abstract*—This paper proposes a novel method to estimate the parameters of isotropic PMSMs which uses only steady-state measurements of load conditions commonly available during the regular operations of off-the-shelf industrial drives. Differently from existing online and offline approaches, the proposed method is designed considering real-world scenarios where ad-hoc tests, additional sensors and the implementation of custom software procedures, such as signal injection, are highly discouraged. The rotor flux linkage, the stator resistance and inductance are estimated with the aid of Adaline neural networks using two operating conditions of the motor. Considering parameter variations according to the actual operating conditions as well as the influence of the inverter nonlinearity and actuation delay, the estimation errors are minimized by proper selecting these two optimal conditions. The accuracy of the proposed method is validated by simulation and experimental studies considering scenarios with different number of motor operating conditions.**

***Index Terms*—Actuation delay compensation, adaline neural network, inverter nonlinearity, large scale application, parameter estimation, rank deficiency, synchronous machines.**

I. Introduction

A. Background

The knowledge of the PMSM parameters, such as inductances, rotor flux linkage, stator resistance, rotor inertia and viscous friction coefficient, is required for several reasons. Most of the common control strategies need the accurate knowledge of the motor parameters to guarantee system stability while ensuring optimal efficiency and dynamic performances [1].

The knowledge of such parameters is also crucial in condition monitoring and fault diagnosis applications as well, e.g., the stator resistance estimation allows to monitor the temperature rise and the winding insulation, while the rotor flux linkage estimation is an indicator of the demagnetization state [2], [3].

The literature reports numerous parameter estimation techniques, mainly divided into offline and online methods [4]. While ensuring high accuracy, offline estimation approaches are based on previously collected input/output data through dedicated tests which need specific laboratory equipment with the motor disconnected from its application [5]. For example, in [6], an offline approach is proposed to estimate the rotor flux linkage using voltage measurements while the PMSM is driven by an induction motor. In [7], several tests in the whole torque-speed range are executed to collect the measurement data required to estimate the motor parameters.

On the other hand, online methodologies do not require the machine to be disconnected as they estimate the parameters during normal on-load operations through real-time implementations on the drive control unit [4]. Online approaches are mainly implemented using numerical methods [8]–[11], state observers [12]–[15], and artificial intelligence techniques [2], [3], [16]. The performances of online approaches are jeopardised by the rank-deficiency issue, i.e., the number of unknown parameters is higher than the rank of the PMSM model, which prevents accurate and simultaneous parameters estimations [3], [17]. Reducing the number of unknown parameters by setting some of them to nominal values is a possible solution [10]. However, while it is not always possible to retrieve nominal values, the convergence of the estimation to the actual values is still not guaranteed [18]. Moreover, variations in operating conditions, aging effects, and incipient faults increase the difference between nominal and actual values, thus adversely affecting the estimation accuracy. More expensive and complex alternatives employ additional measurements, such as those from torque meters [19]. Signal injection (either current, voltage or rotor position offset) represents a further solution to increase the rank of the system [3], [8], [16]. Nevertheless, in case of current or voltage injections, high signal-to-noise ratios must be ensured to provide accurate estimations without influencing the machine parameters [17].

Online methods employ the voltage references in place of measured phase voltages [20]. Hence, the estimation accuracy is additionally compromised due to the mismatch between these two quantities. Such mismatch is mainly due to digital delays and distortions introduced by the control system and by the nonlinearity of the voltage source inverter (VSI) [15]. The VSI nonlinearity can be compensated through an additional parameter in the PMSM model, i.e. the distorted voltage term [21].

While affecting the estimation of the rotor flux linkage

Elia Brescia, Paolo Roberto Massenio, Giuseppe Leonardo Cascella, and Francesco Cupertino are with the Department of Electrical and Information Engineering, Politecnico di Bari, Bari, Italy (e-mail: elia.brescia@poliba.it; paoloroberto.massenio@poliba.it; giuseppeleonardo.cascella@poliba.it; francesco.cupertino@poliba.it).

Mauro Di Nardo and Chris Gerada are with the Power Electronics, Machine and Control Group, University of Nottingham, Nottingham, UK (e-mail: mauro.dinardo4@nottingham.ac.uk; chris.gerada@nottingham.ac.uk).

and stator resistance, the voltage distortion caused by the VSI nonlinearity does not impact the estimation of the q-axis inductance when the d-axis current is null [22]. Instead, as shown in this paper, the digital delay also affects the inductance estimation accuracy and may have a greater impact on the rotor flux linkage and stator resistance estimations. The voltage distortion due to the digital delay increases with the ratio between electrical rotor speed and control sampling frequency, i.e., when high-speed PMSMs or PMSMs with a high number of poles are considered. This is one of the reason of why the main results available in literature of estimation procedures relying on voltage references show experiments at low speeds where the effects of digital delays are negligible [1], [3], [8], [15], [17], [18], [21], [23].

B. Motivation and contributions

Both current online and offline approaches lack of flexibility and nonintrusivity which are a requirement for the condition monitoring of commercial motors in large-scale industrial scenarios. In fact, in these contexts, machine downtimes, dedicated tests and additional measurement devices required by offline methods are highly discouraged. On the other side, effective online approaches relying on signal injection cannot be practically implemented on off-the-shelves commercial drives, as it is usually not allowed to access the drive firmware to implement custom procedures.

The availability of novel Internet-of-Things (IoT) technologies allows for a more flexible and nonintrusive parameter estimation due to the enhanced capability to collect, store and process data. For instance, in [24], an edge/cloud computing architecture has been proposed for the first time to automatically collect and store data generated by in-service PMSMs and to identify the electrical parameters with Adaline Neural Networks (AdNNs). Unfortunately, experimental validation using real measurements is missing in this study. Furthermore, the algorithm in [24] requires a high number of work cycles to estimate the parameters and assumes that voltage measurements are available and that PMSM parameters are constant.

This paper proposes a novel flexible and nonintrusive parameter estimation procedure which overcomes the limitations of both offline and online methods documented so far in the literature. In fact, as in [24], the proposed scheme is designed to operate in a scenario where only data generated during the regular operation of the PMSM are available, without requiring additional sensors. Therefore, only measurements usually available in standard PMSM drives such as rotor position, currents, voltage references, and motor temperature are exploited to provide stator resistance, stator inductance, and rotor flux linkage estimations. Also, to extend the range of applicability, the proposed method is designed to estimate all the parameters by using only two operating conditions. Thereby, the method can be useful also for drives working in few different load/speed steady states. Furthermore, a decision-making algorithm (DMA) has been originally developed to deal with inevitable parameter variations caused by the changing operating conditions. The proposed approach is limited to isotropic PMSM drives under zero d-axis current control, which are by far the most common among PMSM drives in industrial contexts and has been widely studied for the parameter estimation [2], [3], [6], [9], [12], [14], [17]. It has to be remarked that the proposed procedure is not designed to be implemented on the drive control unit, thus, it is suitable for edge/cloud computing architectures capable to collect and store multiple operating conditions. Therefore, typical computational constraints to be considered when designing a real-time algorithm to be embedded in the drive control unit are not present.

Compared to [24], the main novelties and improvements are as follows.

- The algorithm proposed in this paper is more flexible as only two operating conditions are required to estimate the parameters.
- Differently from [24], this paper makes the realistic assumption that the true parameters vary according to the actual operating condition. Indeed, in this paper, the two operating conditions among the collected ones are optimally selected to minimize the estimation errors by considering also the parameter variations.
- Measurement errors are neglected in [24]. Instead, in this work, the influence of the measurement errors on the estimation accuracy is taken into account to support the choice of the optimal operating conditions.
- This work addresses the influence of the inverter nonlinearity and actuation delay on the parameter estimation and proposes a novel compensation method which ensures accuracy also in medium and high frequency applications as well.
- Experimental data are used to validate the proposed approach.

The proposed method is validated with simulation and experimental data considering a high-speed isotropic PMSM drive affected by large parameter variations. In particular, according to the assumptions that ad hoc tests and signal injection cannot be performed, several scenarios with different number of available operating conditions are analyzed to assess the performance of the proposed method.

The rest of the article is organized as follows. Section II reports the adopted PMSM model with digital delays and VSI nonlinearity. Section III details the designed estimation procedure while the simulation and experimental results are presented in Section IV and V, respectively. Finally, Section VI outlines the conclusions of the presented work.

II. PMSM MODEL WITH ACTUATION DELAY AND INVERTER NONLINEARITY

The discrete-time steady-state model of a PMSM in the *dq*-axis reference frame with a zero d-axis current, is [8]:

$$u_{dq}(k) = \begin{bmatrix} u_d(k) \\ u_q(k) \end{bmatrix} = \begin{bmatrix} -L_q \omega(k) i_q(k) \\ R i_q(k) + \psi_m \omega(k) \end{bmatrix}, \tag{1}$$

in which k represents the k-th sample with a sampling period equal to T_s, u_{dq} is the actual dq-axis voltages vector, i_q denotes the q-axis current, ω is the electrical rotor speed, and L_q, R, and ψ_m are the q-axis stator inductance, the

This article has been accepted for publication in IEEE Transactions on Energy Conversion. This is the author's version which has not been fully edited and content may change prior to final publication. Citation information: DOI 10.1109/TEC.2023.3295844

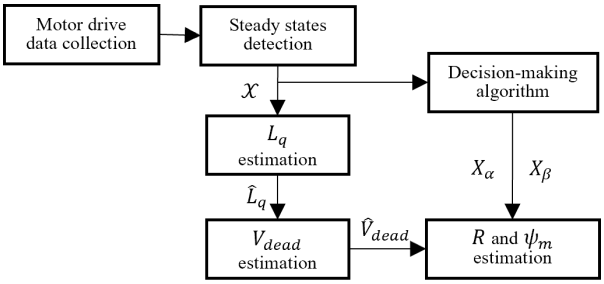

Fig. 1: Information flow of the proposed estimation scheme.

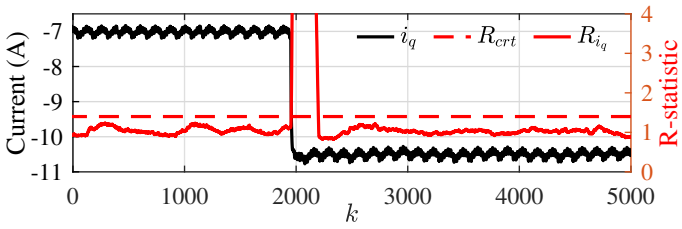

Fig. 2: Detection of the q-axis current steady states.

stator resistance, and the rotor flux linkage, respectively. As previously mentioned, the voltage measurements are not available, and the dq-axis voltage reference u^*_{dq} is employed in place of u_{dq}. However, the voltage references are affected by distortions caused by the digital actuation delay and voltage source inverter (VSI) nonlinearity. The actuation delay is $1.5T_s$ being the sum of the delay due to the digital implementation of the current control T_s and the delay due to the PWM logic $0.5T_s$ [25]. During the actuation delay, $u^*_{dq}((k-1)T_s)$ is fixed in the stationary reference frame while the synchronous frame rotates. Moreover, the VSI nonlinearity introduces additional voltage terms to the voltage references [3].

Therefore, the discrete-time steady-state model need to be corrected to ensure the accuracy of the parameter estimation:

$$\tilde{u}_d(k) = -L_q\omega(k)i_q(k) - D_d(k)V_{dead}, \tag{2a}$$
$$\tilde{u}_q(k) = Ri_q(k) + \psi_m\omega(k) - D_q(k)V_{dead}, \tag{2b}$$

where D_d and D_q are coefficients defined as in [3], V_{dead} is the distorted voltage. Moreover, $\tilde{u}_{dq}$ expresses the voltages with the actuation delay compensation:

$$\tilde{u}_{dq}(k) = \begin{bmatrix} cos(\Delta\theta) & sin(\Delta\theta) \\ -sin(\Delta\theta) & cos(\Delta\theta) \end{bmatrix} u^*_{dq}(k-1), \tag{3}$$

where T_s has been omitted for the sake of brevity and $\Delta\theta$ is the rotor electrical angular shift during the actuation delay that, assuming constant speed, is:

$$\Delta\theta = \frac{3}{2}(\theta(k) - \theta(k-1)). \tag{4}$$

The system of equations (2) includes four parameters to be estimated, i.e., L_q, R, ψ_m, and V_{dead}. However, the rank of this system is two and subsequently at least two operating conditions are required to solve the rank-deficiency issue.

III. Proposed Parameter Estimation

Fig. 1 shows the information flow among the steps of the proposed parameter estimation procedure. The first step is to detect the motor steady states. Next, the estimation of the q-axis inductance and distorted voltage term is carried out. Then, a DMA selects the best operating conditions to estimate the stator resistance and the rotor flux linkage. The following subsections details all the main stages including the rationals behind the DMA.

A. Motor steady states detection

Once the data (speed ω, position θ, dq-axis currents i_{dq}, dq-axis voltage references u^*_{dq} and motor temperature Θ) have been collected, the first step of the proposed approach automatically detects the steady state of i_q and ω adopting the R-statistic method, which computes the following index [26]:

$$R_z(k) = 2\frac{\sum_{i=k-N}^{\infty} z(i)^2 - \frac{1}{N}(\sum_{i=k-N}^{\infty} z(i))^2}{\sum_{i=k-N+1}^{\infty}(z(i) - z(i-1))^2}, \tag{5}$$

where R_z is the index for the generic variable z and N is the length of the moving window. The R-statistic algorithm is designed such that R_z approaches 1 when the variable z is at the steady state. That is, the variable z is claimed to be at the steady state at the k-th step if $R_z(k)$ is lower than a critical threshold R_{crt} (to be chosen slightly greater than one). The tuning of N and R_{crt} can be performed via trial-and-error. The tuned values can be used for different electric drives as they do not depend on specific drive parameters [24]. To better illustrate the working principle of the R-statistic algorithm, Fig. 2 shows the detection of two different steady states of the q-axis current of a real motor. The sample time is $T_s = 25\mu$s while $R_{crt} = 1.4$ and $N = 250$. It can be seen how the R-statistic algorithm detects the perturbation of the steady state during an abrupt load change and approaches again the unity when the transient state has ended.

The R-statistic method is exploited to extract the motor operating conditions (OCs) according to Algorithm 1. In this algorithm, k_{lim} and $\Delta\Theta_{lim}$ are tuning parameters that allow to define the OCs time extension and temperature range. Instead, i and k_i are indexes initialized to one. The set of the N_s extracted OCs is defined as $\mathcal{X} = \{X_1, \ldots, X_{N_s}\}$, where X_i, $i = 1, \ldots, N_s$, contains the steady-state data of the i-th OC, as follows:

$$\begin{aligned} X_i = \{&\omega_i(1), \ldots, \omega_i(N_i), i_{q_i}(1), \ldots, i_{q_i}(N_i), \\ &\tilde{u}_{dq_i}(1), \ldots, \tilde{u}_{dq_i}(N_i), D_{d_i}(1), \ldots, D_{d_i}(N_i), \\ &D_{q_i}(1), \ldots, D_{q_i}(N_i), \Theta_i(1), \ldots, \Theta_i(N_i)\}, \end{aligned} \tag{6}$$

where N_i is the number of samples in the i-th OC, Θ_i denotes the motor temperature, and $\tilde{u}_{dq_i}$, D_{d_i}, D_{q_i} are computed using the measured data according to (3), (4), and [3].

B. L_q and V_{dead} estimation

The inductance in each OC, L_{q_i}, is estimated using an AdNN, whose general structure and working principle is detailed in Appendix A. The estimated q-axis inductance $\hat{L}^w_{q_i}$, $i = 1, \ldots, N_s$ is the weight of the AdNN, the compensated

Algorithm 1 OCs extraction

Input: $\Theta(k)$, $R_{i_q}(k)$, $R_\omega(k)$, k_{lim}, $\Delta\Theta_{lim}$.
Output: X_i

If $R_{i_q}(k) < 1$ **and** $R_\omega(k) < 1$
  If $k_i = 1$ **or** ($k_i < k_{lim}$ **and** $|\Theta_i(1) - \Theta(k)| < \Delta\Theta_{lim}$)
    a. Set $\omega_i(k_i) = \omega(k)$, $i_{q_i}(k_i) = i_q(k)$, $\tilde{u}_{dq_i}(k_i) = \tilde{u}_{dq}(k)$, $D_{d_i}(k_i) = D_d(k)$, $D_{q_i}(k_i) = D_q(k)$, $\Theta_i(k_i) = \Theta(k)$;
    b. Set $k_i = k_i + 1$.
  else
    Set $N_i = k_{i-1}$, $i = i + 1$, $k_i = 1$.
else
  If $R_{i_q}(k-1) < 1$ **and** $R_\omega(k-1) < 1$
    Set $N_i = k_{i-1}$, $i = i + 1$, $k_i = 1$
  else
    Set $i = i$, $k_i = 1$

d-axis voltage $\tilde{u}_{d_i}$ is the measured output, the estimated d-axis voltage $\hat{u}_{d_i}$ is the network's output, and the bias is set equal to zero. The inductance estimation is updated as follows:

$$\begin{aligned}\hat{L}^w_{q_i}(k) &= \hat{L}^w_{q_i}(k-1) - 2\eta_L\omega_i(k)i_{q_i}(k)\left(\tilde{u}_{d_i}(k) - \hat{u}_{d_i}(k)\right),\\ \hat{u}_{d_i}(k) &= -\omega(k)i_{q_i}(k)\hat{L}^w_{q_i}(k-1),\end{aligned} \tag{7}$$

where $k = 1, \ldots, N_i$, and η_L is the learning rate that can be dynamically adjusted to regulate the convergence speed, see Appendix A for a detailed analysis. The estimated inductance, $\hat{L}_{q_i}$, is set to the final network weight, i.e., $\hat{L}_{q_i} = \hat{L}^w_{q_i}(N_i)$. It is worth underlining that the estimation of L_{q_i} can be performed without knowing the term V_{dead_i} even though is based on (2a). In fact, since the coefficient D_{d_i} has zero-mean when $i_d = 0$, it does not affect the estimation of L_{q_i} if $\hat{L}^w_{q_i}$ is filtered [3]. The impact of measurements error on the estimated inductance is analyzed in Appendix B.

For each OC, once $\hat{L}_{q_i}$ has been computed, the estimation of the corresponding V_{dead_i} is obtained by means of an optimization problem based on (2a):

$$\min_{\hat{V}_{dead_i}} \sum_{k=N_i-N_{si}+1}^{N_i}(D_{d_i}(k)\hat{V}_{dead_i} + \tilde{u}_{d_i}(k) + \hat{L}_{q_i}\omega_i(k)i_{q_i}(k)))^2, \tag{8}$$

where $N_{si} = \frac{2\pi}{6\omega_i T_s}$ represents the number of available samples in a period of the function $D_{d_i}(k)\hat{V}_{dead_i}$ [3]. Note that the estimation of the distorted voltage is particularly challenging as it is based on the harmonic content of the d-axis equation (D_{d_i} has zero mean) which can be corrupted by noise and measurement errors [3]. Furthermore, the accuracy of the solution of this optimization problem depends on N_{si} as the availability of a high number of samples increases the optimization robustness, especially with respect to measurement errors and additional phenomena not considered in (2a).

C. R and ψ_m estimation

As previously mentioned, to overcome the rank-deficiency issue of (2b), two different OCs among those collected are used to estimate both R and ψ_m. The first OC, $\alpha \in \{1, \ldots, N_s\}$, feeds an AdNN, i.e. AdNN1, for the estimation of ψ_m, while the second OC, $\beta \in \{1, \ldots, N_s\} \setminus \{\alpha\}$, feeds a second Adaline NN, i.e. AdNN2, for the estimation of R. Due to their simplicity, accuracy, and low computational burden, AdNNs have also been used in [2] and [3] to estimate the stator resistance and rotor flux linkage. However, note that in these works the AdNNs have been designed by considering a modified steady-state model of the PMSM with the signal injection, which simplifies the solution of the rank-deficient problem. Instead, in the present work, the rank-deficient problem has been originally solved with two AdNNs based on the model of the PMSM without signal injection.

Given the data of the two selected OCs, i.e. X_α and X_β, the estimations of ψ_m and R, i.e., $\hat{R}^*$, $\hat{\psi}^*_m$, are obtained according to Algorithm 2, which outlines the coupling procedure of the two networks. First, the provisional estimations of both ψ_m and R are initialized to zero and both rotor flux linkage and stator resistance estimations can be performed at the first iteration. The estimation of ψ_m (step 2) is provided by AdNN1 based on the followings:

$$\begin{aligned}\hat{\psi}^w_m(k) &= \hat{\psi}^w_m(k-1) + \\ &+ 2\eta_\psi\omega_\alpha(k)\left(\tilde{u}_{q_\alpha}(k) + D_{q_\alpha}(k)\hat{V}_{dead_\alpha} - \hat{u}_{q_\alpha}(k)\right),\\ \hat{u}_{q_\alpha}(k) &= \hat{R}^{*^{(j-1)}}i_{q_\alpha}(k) + \omega_\alpha(k)\hat{\psi}^w_m(k-1),\end{aligned} \tag{9}$$

where η_ψ is the learning rate and $\hat{R}^{*^{(j-1)}}$ is the estimated stator resistance at the j-th iteration. According to Appendix A, $\hat{\psi}^w_m$ is the weight, $\tilde{u}_{q_\alpha}$ is the measured output, $\hat{u}_{q_\alpha}$ is the estimated output, ω_α is the input and $\hat{R}^{*^{(j-1)}}i_{q_\alpha}$ is the bias.

Analogously, the estimation of R (step 3) is provided by AdNN2:

$$\begin{aligned}\hat{R}^w(k) &= \hat{R}^w(k-1) + \\ &+ 2\eta_R i_{q_\beta}(k)(\tilde{u}_{q_\beta}(k) + D_{q_\beta}(k)\hat{V}_{dead_\beta} - \hat{u}_{q_\beta}(k)),\\ \hat{u}_{q_\beta}(k) &= \hat{R}^w(k)i_{q_\beta}(k) + \omega_\beta(k)\hat{\psi}^{*^{(j)}}_m,\end{aligned} \tag{10}$$

where η_R is the learning rate and $\hat{\psi}^{*^{(j)}}_m$ is the estimated rotor flux linkage at the j-th iteration. Let's underline that the provisional estimations are set equal to the last values provided by AdNN1 and AdNN2 at the j-th iteration. As mentioned for η_L, also η_ψ and η_R can be dynamically adjusted to ensure the convergence of AdNN1 and AdNN2. The steps 2 and 3 of Algorithm 2 are repeated until the following stop criterion is satisfied:

$$\left|\frac{\hat{\psi}^{*^{(j)}}_m - \hat{\psi}^{*^{(j-1)}}_m}{\hat{\psi}^{*^{(j)}}_m}\right| + \left|\frac{\hat{R}^{*^{(j)}} - \hat{R}^{*^{(j-1)}}}{\hat{R}^{*^{(j)}}}\right| < \epsilon, \tag{11}$$

where ϵ is a small threshold.

D. Convergence analysis

In the following subsection, the convergence properties of the proposed Algorithm 2 is analysed to determine the criteria of the selection of the OCs used to estimate both resistance and

Algorithm 2 Operation of the coupled Adaline NNs

Input: X_α, X_β, V_{dead_α}, V_{dead_β}.
Output: Estimations $\hat{R}^*$, $\hat{\psi}_m^*$

1: **Provisional estimations initialization**
Set $\hat{R}^{*^{(0)}} = 0$, $\hat{\psi}_m^{*^{(0)}} = 0$, and $j = 1$.
2: **Rotor flux linkage estimation**
a. Set $\hat{\psi}_m^w(0) = \hat{\psi}_m^{*^{(j-1)}}$;
b. Compute $\hat{\psi}_m^w(k)$, with $k = 1, \ldots, N_\alpha$, as in (9);
c. Set $\hat{\psi}_m^{*^{(j)}} = \hat{\psi}_m^w(N_\alpha)$.
3: **Stator resistance estimation**
a. Set $\hat{R}^w(0) = \hat{R}^{*^{(j-1)}}$;
b. Compute $\hat{R}^w(k)$, with $k = 1, \ldots, N_\beta$, as in (10);
c. Set $\hat{R}^{*^{(j)}} = \hat{R}^w(N_\beta)$.
4: **Stop Criterion**
if (11) is satisfied then return $\hat{R}^* = \hat{R}^{*^{(j)}}$ and $\hat{\psi}_m^* = \hat{\psi}_m^{*^{(j)}}$. Otherwise, set $j = j + 1$ and go back to step 2.

rotor flux linkage. Indeed, by solving the difference equation in (9), it results that:

$$\psi_m^w(k) = c\left(1 - 2\eta_\psi \omega_\alpha(k)^2\right)^k + \frac{\tilde{u}_{q_\alpha}(k) + D_{q_\alpha}(k)\hat{V}_{dead_\alpha} - \hat{R}^{*^{(j-1)}} i_{q_\alpha}(k)}{\omega_\alpha(k)}, \quad (12)$$

where c is a real constant. We assume that the AdNN1 is at the steady state at the sample N_α, thus at the j-th iteration of Algorithm 2:

$$\hat{\psi}_m^{*^{(j)}} = \hat{\psi}_m^w(N_\alpha) = \frac{\bar{\tilde{u}}_{q_\alpha} + \bar{D}_{q_\alpha}\hat{V}_{dead_\alpha} - \hat{R}^{*^{(j-1)}}\bar{i}_{q_\alpha}}{\bar{\omega}_\alpha}, \quad (13)$$

where the generic variable $\bar{x}_\alpha$ stands for $x_\alpha(N_\alpha)$. By evaluating (2b) in $k = N_\alpha$ and assuming $V_{dead_\alpha} \approx \hat{V}_{dead_\alpha}$ it follows:

$$\bar{\tilde{u}}_{q_\alpha} + \bar{D}_{q_\alpha}\hat{V}_{dead_\alpha} = R_\alpha \bar{i}_{q_\alpha} + \psi_{m_\alpha}\bar{\omega}_\alpha, \quad (14)$$

where R_α and ψ_{m_α} are the actual values of the stator resistance and rotor flux linkage in the OC α and at the sample N_α. Then, substituting (14) in (13) provides:

$$\hat{\psi}_m^{*^{(j)}} = \frac{R_\alpha \bar{i}_{q_\alpha} + \psi_{m_\alpha}\bar{\omega}_\alpha - \hat{R}^{*^{(j-1)}}\bar{i}_{q_\alpha}}{\bar{\omega}_\alpha}. \quad (15)$$

Analogously, the stator resistance in the OC β estimated at the $(j-1)$-th iteration is:

$$\hat{R}^{*^{(j-1)}} = \frac{R_\beta \bar{i}_{q_\beta} + \psi_{m_\beta}\bar{\omega}_\beta - \hat{\psi}_m^{*^{(j-1)}}\bar{\omega}_\beta}{\bar{i}_{q_\beta}}, \quad (16)$$

where R_β and ψ_{m_β} are the actual values of the stator resistance and rotor flux linkage in the OC β and at the sample N_β. By substituting (16) in (15), the following first-order difference equation is obtained:

$$\hat{\psi}_m^{*^{(j)}} = \psi_{m_\alpha} + \left(R_\alpha - R_\beta + \left(\hat{\psi}_m^{*^{(j-1)}} - \psi_{m_\beta}\right)\frac{\bar{\omega}_\beta}{\bar{i}_{q_\alpha}}\right)\frac{\bar{i}_{q_\beta}}{\bar{\omega}_\alpha}, \quad (17)$$

whose solution is:

$$\hat{\psi}_m^{*^{(j)}} = cr^j + \hat{\psi}_m^{*^{(\infty)}}, \quad j \geq 1, \quad (18)$$

where c is a real constant, $r = \frac{\bar{i}_{q_\alpha}\bar{\omega}_\beta}{\bar{i}_{q_\beta}\bar{\omega}_\alpha}$, and

$$\hat{\psi}_m^{*^{(\infty)}} = \frac{\psi_{m_\alpha} - \psi_{m_\beta} r}{1 - r} + (R_\alpha - R_\beta)\frac{\frac{\bar{i}_{q_\beta}}{\bar{\omega}_\alpha}}{1 - r}, \quad (19)$$

is the steady-state value of (17). By substituting (18) in (16), the following holds true:

$$\hat{R}^{*^{(j)}} = -c\frac{\bar{\omega}_\beta}{\bar{i}_{q_\beta}} r^j + \hat{R}^{*^{(\infty)}}, \quad j \geq 1, \quad (20)$$

where

$$\hat{R}^{*^{(\infty)}} = \frac{R_\beta - R_\alpha r}{1 - r} + (\psi_{m_\beta} - \psi_{m_\alpha})\frac{\frac{\bar{\omega}_\beta}{\bar{i}_{q_\beta}}}{1 - r}, \quad (21)$$

is the steady-state value of $\hat{R}^{*^{(j)}}$.

Considering (18) and (20), which express the estimation of the resistance and rotor flux linkage at the j-th step, it is clear that to ensure the convergence of the estimations, the OCs α and β must be selected in order to satisfy the following condition:

$$|r| = \left|\frac{\bar{i}_{q_\alpha}\bar{\omega}_\beta}{\bar{i}_{q_\beta}\bar{\omega}_\alpha}\right| < 1. \quad (22)$$

In other words, for a given OC α, not all OCs β guarantee the convergence of the coupled AdNNs. Note that the value of r also affects the estimation convergence speed, i.e. the number of iterations required to satisfy the stop criterion (11). If the convergence condition in (22) is satisfied, then the results of Algorithm 2 are expressed by (19) and (21). In particular, (21) can be expressed in the two following forms:

$$\begin{aligned} \hat{R}^{*^{(\infty)}} &= R_\alpha + \varepsilon_{R_\alpha}, \\ \hat{R}^{*^{(\infty)}} &= R_\beta + \varepsilon_{R_\beta}, \end{aligned} \quad (23)$$

where

$$\begin{aligned} \varepsilon_{R_\alpha} &= \frac{R_\beta - R_\alpha}{1 - r} + \frac{(\psi_{m_\beta} - \psi_{m_\alpha})\frac{\bar{\omega}_\beta}{\bar{i}_{q_\beta}}}{1 - r}, \\ \varepsilon_{R_\beta} &= \frac{(R_\beta - R_\alpha)r}{1 - r} + \frac{(\psi_{m_\beta} - \psi_{m_\alpha})\frac{\bar{\omega}_\beta}{\bar{i}_{q_\beta}}}{1 - r}. \end{aligned} \quad (24)$$

In other words, the stator resistance estimation can be expressed as the actual stator resistance in the OC α or β plus a systematic estimation error (ε_{R_α}, ε_{R_β}), caused by the mismatch of ψ_m and R in the two OCs. The same results holds for the rotor flux linkage estimation:

$$\begin{aligned} \hat{\psi}_m^{*^{(\infty)}} &= \psi_{m_\alpha} + \varepsilon_{\psi_{m_\alpha}}, \\ \hat{\psi}_m^{*^{(\infty)}} &= \psi_{m_\beta} + \varepsilon_{\psi_{m_\beta}}, \end{aligned} \quad (25)$$

where

$$\begin{aligned} \varepsilon_{\psi_\alpha} &= \frac{(\psi_{m_\alpha} - \psi_{m_\beta})r}{1 - r} + \frac{(R_\alpha - R_\beta)\frac{\bar{i}_{q_\beta}}{\bar{\omega}_\alpha}}{1 - r}, \\ \varepsilon_{\psi_\beta} &= \frac{(\psi_{m_\alpha} - \psi_{m_\beta})}{1 - r} + \frac{(R_\alpha - R_\beta)\frac{\bar{i}_{q_\beta}}{\bar{\omega}_\alpha}}{1 - r}. \end{aligned} \quad (26)$$

It is clear that, when considering an ideal PMSM whose parameters are constant, then $\psi_{m_\alpha} = \psi_{m_\beta} = \psi_m$ and $R_\alpha = R_\beta = R$ and the estimations would be affected only

by measurement errors, which are detailed in Appendix B. However, in a real PMSM, the parameters vary with the OC (e.g. due to the temperature or the frequency effects) and the errors expressed by (24) and (26) cannot be neglected. The DMA, described in the following subsection, chooses the two OCs α and β among the collected ones to estimate both resistance and rotor flux linkage in order to minimize these systematic estimation errors.

E. Decision-Making Algorithm

First, for any collected OC α and β, with $\alpha \neq \beta$, the majorants of the systematic errors in (24) and (26) are approximately computed as follows:

$$\begin{aligned}\tilde{\varepsilon}_{R_\alpha} &= \left|\frac{\tilde{R}_\beta - \tilde{R}_\alpha}{1-r}\right| + \left|\frac{(\tilde{\psi}_{m_\beta} - \tilde{\psi}_{m_\alpha})\frac{\bar{\omega}_\beta}{\bar{i}_{q_\beta}}}{1-r}\right|,\\ \tilde{\varepsilon}_{R_\beta} &= \left|\frac{(\tilde{R}_\beta - \tilde{R}_\alpha)r}{1-r}\right| + \left|\frac{(\tilde{\psi}_{m_\beta} - \tilde{\psi}_{m_\alpha})\frac{\bar{\omega}_\beta}{\bar{i}_{q_\beta}}}{1-r}\right|,\end{aligned} \tag{27}$$

$$\begin{aligned}\tilde{\varepsilon}_{\psi_\alpha} &= \left|\frac{(\tilde{\psi}_{m_\alpha} - \tilde{\psi}_{m_\beta})r}{1-r}\right| + \left|\frac{(\tilde{R}_\alpha - \tilde{R}_\beta)\frac{\bar{i}_{q_\alpha}}{\bar{\omega}_\alpha}}{1-r}\right|,\\ \tilde{\varepsilon}_{\psi_\beta} &= \left|\frac{\tilde{\psi}_{m_\alpha} - \tilde{\psi}_{m_\beta}}{1-r}\right| + \left|\frac{(\tilde{R}_\alpha - \tilde{R}_\beta)\frac{\bar{i}_{q_\alpha}}{\bar{\omega}_\alpha}}{1-r}\right|,\end{aligned} \tag{28}$$

where $\tilde{R}_\iota$ and $\tilde{\psi}_{m_\iota}$ are the initial estimations of R_ι and ψ_{m_ι}, respectively, with $\iota = \alpha, \beta$. Such initial estimations are computed using only the available temperature and speed information related to the OCs. In particular, both resistance and rotor flux linkage are supposed to depend from temperature and frequency according to the following laws [27], [28]:

$$\tilde{R}_\iota = \hat{R}_0\left(1 + \alpha_0(\bar{\Theta}_\iota - 20)\right)\left(1 + \tilde{\beta}_0\left(\frac{\bar{\omega}_\iota}{2\pi}\right)^2\right), \tag{29}$$

$$\tilde{\psi}_{m_\iota} = \hat{\psi}_0\left(1 + \tilde{\alpha}_{PM0}(\bar{\Theta}_\iota - 20)\right), \tag{30}$$

where $\tilde{R}_\iota$ depends on both frequency and temperature while $\tilde{\psi}_{m_\iota}$ depends only on the temperature. In these relationships, $\alpha_0 = 0.393\%/°\text{C}$ is the copper temperature coefficient while $\tilde{\beta}_0$ and $\tilde{\alpha}_{PM0}$ are the supposed frequency coefficient and PM temperature coefficient, respectively. Considering that the PM temperature coefficient $\tilde{\alpha}_{PM0}$ is generally in the interval $[-0.2; -0.02]$ $\%/°\text{C}$, for the supposed coefficient it is set $\tilde{\alpha}_{PM0} = -0.1\%/°\text{C}$ as a trade-off value. Instead, to set the value of $\tilde{\beta}_0$, a precautionary hypothesis is that the stator resistance at rated speed is at most ten times the stator resistance at zero speed. Therefore, $\tilde{\beta}_0$ can be approximately calculated as:

$$\tilde{\beta}_0 \approx \frac{9}{(\frac{\omega_r}{2\pi})^2}. \tag{31}$$

with ω_r denoting the electrical rated speed. The values of $\hat{R}_0$ and $\hat{\psi}_0$, i.e. the stator resistance and rotor flux linkage estimations at zero speed and 20°C, required to compute (29) and (30), are obtained by leveraging Algorithm 2. In particular, for $\hat{R}_0$, the OC β closest to zero speed and 20°C is selected:

$$\beta = \underset{i=1,\dots,N_s}{argmin}\left|1 - \left(1 + \alpha_0(\bar{\Theta}_i - 20)\right)\left(1 + \beta_0\left(\frac{\bar{\omega}_\iota}{2\pi}\right)^2\right)\right|, \tag{32}$$

then, the OC α is chosen such that r is minimized:

$$\alpha = \underset{\substack{i=1,\dots,N_s\\ i\neq\beta}}{argmin}\left|\frac{\bar{i}_{q_i}\bar{\omega}_\beta}{\bar{i}_{q_\beta}\bar{\omega}_i}\right|. \tag{33}$$

Once α and β are defined, Algorithm 2 estimates $\hat{R}^*$, thus $\hat{R}_0$ is computed as:

$$\hat{R}_0 = \frac{\hat{R}^*}{\left(1 + \alpha_0(\bar{\Theta}_\beta - 20)\right)\left(1 + \beta_0\left(\frac{\bar{\omega}_\iota}{2\pi}\right)^2\right)}. \tag{34}$$

In a similar way, for $\hat{\psi}_0$, the OC α closest to 20°C is chosen:

$$\alpha = \underset{i=1,\dots,N_s}{argmin}\left|\bar{\Theta}_i - 20\right|, \tag{35}$$

then, the OC β is selected always minimizing the index r:

$$\beta = \underset{\substack{i=1,\dots,N_s\\ i\neq\alpha}}{argmin}\left|\frac{\bar{i}_{q_\alpha}\bar{\omega}_i}{\bar{i}_{q_i}\bar{\omega}_\alpha}\right|. \tag{36}$$

Using the selected OCs α and β, Algorithm 2 finds $\hat{\psi}^*_m$, therefore $\hat{\psi}_0$ is computed as:

$$\hat{\psi}_0 = \frac{\hat{\psi}^*_m}{1 + \alpha_{PM0}(\bar{\Theta}_\alpha - 20)}. \tag{37}$$

It has to be underlined that the just described procedure does not require any information about the PMSM to identify but requires to make hypothesis on the values of the coefficients, $\tilde{\beta}_0$ and $\tilde{\alpha}_{PM0}$. Once $\hat{R}_0$ and $\hat{\psi}_0$ are computed, for each OC i (hereafter called main operating condition MOC), the DMA finds an auxiliary operating condition (AOC) which minimizes the estimation error of the stator resistance in MOC, i.e., $\hat{R}_i$. As detailed in Algorithm 3, candidates AOCs coupled with the considered MOC are those which ensure convergence, i.e., $r < \varepsilon_r$, with $\varepsilon_r < 1$ as a threshold. In particular, ε_r should be selected as a trade-off between the estimability and the accuracy of the estimation. In fact, a small value of ε_r could make impossible to find an AOC while a value of r near to one would amplify the estimation error caused by the measurement, as shown in Appendix B. Adopting this approach, the estimation error is not limited, therefore it is further capped rejecting estimations whose majorants (27) are bigger than 25% of the initial stator resistance estimation (29). The same procedure applies to the rotor flux linkage estimation by substituting $\tilde{\varepsilon}_{R_\alpha}$, $\tilde{\varepsilon}_{R_\beta}$, $\tilde{R}_\alpha$, $\tilde{R}_\beta$ with $\tilde{\varepsilon}_{\psi_\alpha}$, $\tilde{\varepsilon}_{\psi_\beta}$, $\tilde{\psi}_{m_\alpha}$, $\tilde{\psi}_{m_\beta}$, and (27) with (28) in Algorithm 3. Once the AOC is found, Algorithm 2 computes the actual estimations. The complete procedure for the stator resistance and rotor flux linkage estimation in each OC is in Algorithm 4.

Algorithm 3 DMA for resistance estimations

Input: OC i, $\hat{R}_0$, $\hat{\psi}_0$, ε_r.
Output: OCs α, β.

1: **Sets definition**
Determine

$$\mathcal{X}_\beta^{'} = \{j \in \{1,\dots,N_s\} \ s.t. \ r < \varepsilon_r \ and \ \tilde{\varepsilon}_{R_\alpha} < \frac{\tilde{R}_\alpha}{4} \ with \ \alpha = i, \beta = j\}$$

$$\mathcal{X}_\alpha^{'} = \{j \in \{1,\dots,N_s\} \ s.t. \ r < \varepsilon_r \ and \ \tilde{\varepsilon}_{R_\beta} < \frac{\tilde{R}_\beta}{4} \ with \ \alpha = j, \beta = i\}$$

where $\tilde{\varepsilon}_{R_\alpha}$, $\tilde{\varepsilon}_{R_\beta}$ are as in (27) and $\tilde{R}_\alpha$, $\tilde{R}_\beta$ are computed using $\hat{R}_0$, $\hat{\psi}_0$.
2: **if** $\mathcal{X}_\beta^{'} \neq \emptyset$ **then**
Find $j_1 \in \mathcal{X}_\beta^{'}$ corresponding to the minimum value of $\tilde{\varepsilon}_{R_\alpha}$, then set $\varepsilon_1 = \tilde{\varepsilon}_{R_\alpha}$, with $\alpha = i$, $\beta = j_1$.
else
Set $\varepsilon_1 = \infty$
3: **if** $\mathcal{X}_\alpha^{'} \neq \emptyset$ **then**
Find $j_2 \in \mathcal{X}_\alpha^{'}$ corresponding to the minimum value of $\tilde{\varepsilon}_{R_\beta}$, then set $\varepsilon_2 = \tilde{\varepsilon}_{R_\beta}$, with $\alpha = j_2$, $\beta = i$.
else
Set $\varepsilon_2 = \infty$
4: **if** $\varepsilon_1 < \infty$ **or** $\varepsilon_2 < \infty$ **then**
if $\varepsilon_1 > \varepsilon_2$ **then**
Set $\alpha = j_2$, $\beta = i$
else
Set $\alpha = i$, $\beta = j_1$
return α, β.
else
Estimation rejected.

Algorithm 4 Resistance and rotor flux linkage estimation

Input: OC i.
Output: Estimated parameters in the OC i ($\hat{R}_i$, $\hat{\psi}_{m_i}$).

1: **Resistance estimation**
a. Run DMA for resistance estimation and obtain α, β.
b. Run Algorithm 2 and set $\hat{R}_i = \hat{R}^*$.
2: **Rotor flux linkage estimation**
a. Run DMA for rotor flux linkage estimation and obtain α, β.
b. Run Algorithm 2 and set $\hat{\psi}_{m_i} = \hat{\psi}_m^*$.

IV. Simulation results

The proposed estimation method has been tested using both experimental and simulation data considering a PMSM drive whose main parameters are reported in Table I. The values of the parameters reported in this table are obtained using experimental procedures and measurement devices. In particular, the inductances and rotor flux linkage are obtained by means of the experimental procedure described in [20]. The inductances can be considered constants as the machine does not operate in saturated condition. Instead, the stator resistance has been measured using an ohmmeter.

TABLE I: PMSM drive parameters

Parameter	Value	Unit
Rated power	4.2	kW
Rated speed	80	krpm
Rated Current	7	A
DC link voltage	540	V
Number of pole pairs	2	
R_0	0.6975	Ω
ψ_{m0}	26.82	mWb
L_d	1.251	mH
L_q	1.251	mH
α_0	0.393	$\%/^\circ C$
α_{PM0}	-0.035	$\%/^\circ C$
Drain-source on-state voltage $V_{ds(on)}$	0.1	V
Freewheeling diode forward voltage V_d	2	V
T_s	25	μs
Active switches turn on time T_{on}	65	ns
Active switches turn off time T_{off}	300	ns

The simulations have been performed in Matlab/Simulink environment replicating as much as possible the conditions of the experimental tests, which are detailed in the next section. Indeed, the resistance used in the PMSM model changes with the operating condition according to the following law:

$$R = R_{AC}|_{20}(\omega)[1 + \alpha_0(\Theta - 20)], \tag{38}$$

where $R_{AC}|_{20}(\omega)$ is a 1-D look-up containing the AC stator resistance measurements at 20 °C, while the rotor flux linkage changes as:

$$\psi_m = \psi_{m0}\left(1 + \alpha_{PM0}(\Theta - 20)\right), \tag{39}$$

with the values of ψ_0 and α_{PM0} listed in Table I. Note that the value of β_0 that fits the experimental measurements $R_{AC}|_{20}$ is approximately equal to $3.52 \cdot 10^{-7}$/Hz^2 while, according to (31), it is set $\tilde{\beta}_0 = 1.0 \cdot 10^{-6}$/Hz^2. The inverter distorted voltage is kept constant during the simulations ($V_{dead} = 0.35$V).

To validate the proposed method, a set of twenty OCs is considered, each one with 5000 samples and constant temperature, which are shown in Table II. It has to be noted that the high temperature and frequency variations among the collected OCs make particularly difficult the problem of accurately estimating the PMSM parameters.

Fig. 3 illustrates the dynamics of the AdNNs during the estimations of q-axis inductance, stator resistance, and rotor flux linkage in the OC 6. The x-axes of the figures report the number of samples processed by the AdNNs. For instance, in Fig. 3(d), 100 samples are shown which correspond to a time window of 2.5ms, according to the sampling time in Table I. Such a time window does not coincide with the computational time as the proposed algorithm has been implemented in an offline fashion. In Fig. 3 (a) and (c), two cases are shown with AOC set equal to OC 2 ($r = 0.2$) and OC 5 ($r = 0.5$), respectively. Note how the convergence speed is influenced by the value of r and how the AOCs impact the estimation accuracy. Instead, Fig. 3 (b) shows the non convergence of the estimation when selecting a couple of OCs which do not satisfy the condition (22). Finally, Fig. 3(d) shows the inductance estimation dynamics with two different learning rate values corresponding to $\lambda = 0.95$ and $\lambda = 0.5$.

This article has been accepted for publication in IEEE Transactions on Energy Conversion. This is the author's version which has not been fully edited and content may change prior to final publication. Citation information: DOI 10.1109/TEC.2023.3295844

TABLE II: Collected OCs

OC	$\bar{i}_q$ [A]	$\bar{\Omega}$ [krpm]	$\bar{\Theta}$ [°C]	OC	$\bar{i}_q$ [A]	$\bar{\Omega}$ [krpm]	$\bar{\Theta}$ [°C]
1	3.5	6	33	11	10.5	18	75
2	7	6	46	12	14	18	115
3	10.5	6	70	13	3.5	24	39
4	14	6	112	14	7	24	51
5	3.5	12	36	15	10.5	24	74
6	7	12	49	16	14	24	113
7	10.5	12	73	17	3.5	30	43
8	14	12	114	18	7	30	55
9	3.5	18	39	19	10.5	30	78
10	7	18	52	20	14	30	119

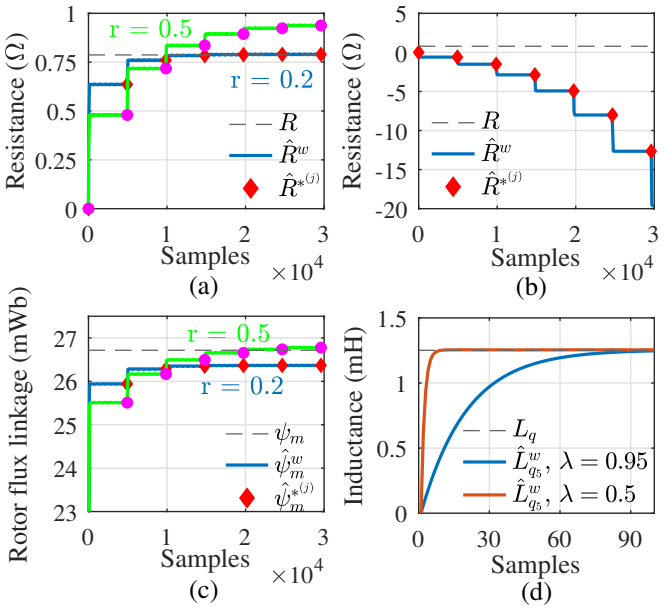

Fig. 3: Estimation dynamics related to OC 6: (a) stator resistance ($r < 1$), (b) stator resistance ($r > 1$), (c) rotor flux linkage $r < 1$, and (d) q-axis inductance.

It is evident that few samples are required to obtain the convergence when small values of λ are chosen.

A. Effect of the inverter nonlinearity compensation

Fig. 4 shows the comparison between the voltage references, the compensated voltages ($\tilde{u}_{dq}$), the compensated voltages with the compensation of the VSI nonlinearity ($\tilde{u}_{dq} + D_{dq}\hat{V}_{dead}$), and the actual voltages applied to the PMSM in three different OCs. As expected, these figures show that the errors between the actual voltages and the voltage references increase with the speed. In particular, the results reveal that the main cause of the voltage distortion is the actuation delay, which affects the dq-axis voltages. In fact, the error between u_d^* and $\tilde{u}_d$ can exceed 35 V while the error between u_q^* and $\tilde{u}_q$ can overcome 8 V. It can also be inferred that the voltage distortion caused by the VSI nonlinearity affects only the q-axis voltage. All these errors can be substantially reduced thanks to the proposed actuation delay and VSI nonlinearity compensation.

B. Inductance and distorted voltage term estimations

In Table III, the results of the estimation of the q-axis inductance and distorted voltage in all the collected OCs

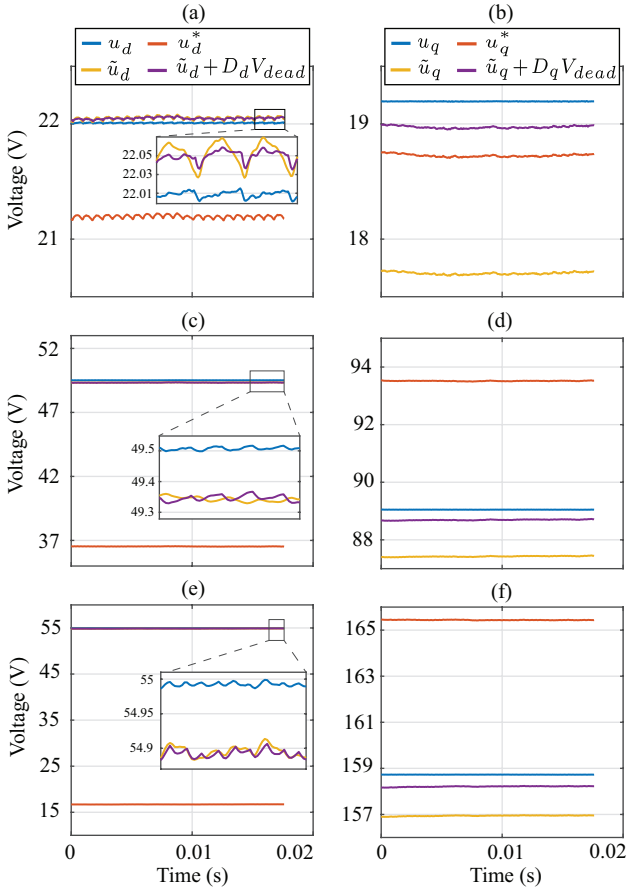

Fig. 4: d-axis voltages in OC 4 (a), 11 (c), 18 (e) and q-axis voltages in OC 4 (b), 11 (d), 18 (f).

are reported. Thanks to the actuation delay compensation, a high accuracy of the estimation of the q-axis inductance is achieved with an average absolute error of 0.64%. The same table also lists the actual estimation error achieved without compensating (last column) the actuation delay. It is clear that the compensation of the latter is fundamental in obtaining an accurate estimation.

Regarding the distorted voltage estimation, satisfactory results have been obtained although the estimation accuracy gets worse with the increase of the motor speed (lowest speeds OCs 1-4, highest speeds OCs 17-20). In fact, since the sample time is fixed, the speed increase causes the reduction of samples in a period of $D_{d_i}(k)\hat{V}_{dead_i}$ which in turn affects the effectiveness of the optimization (8).

C. Resistance and rotor flux linkage estimations

Fig. 5 reports the results of the estimation of ψ_m and R using Algorithm 4 and considering several scenarios with different number of available OCs. For each scenario s, N_s different tests are performed by randomly choosing k_s OCs among $\mathcal{X}$, with $k_s = 1, 2, ..., 6$. Note that, as the whole dataset contains 20 OCs, the number of combinations of OCs without repetition when k_s OCs are available is given by:

$$N_{comb_s} = \frac{20!}{k_s!(20-k_s)!}. \quad (40)$$

TABLE III: Inductance and distorted voltage term estimations

OC	L_q [mH]	$\hat{L}_q$ [mH]	Actual error [%]	V_{dead} [V]	$\hat{V}_{dead}$ [V]	Actual error n.c. [%]
1	1.251	1.251	<0.01	-0.350	-0.319	25.78
2	1.251	1.251	0.03	-0.350	-0.317	11.53
3	1.251	1.254	0.20	-0.350	-0.413	6.47
4	1.251	1.255	0.28	-0.350	-0.462	3.62
5	1.251	1.264	1.00	-0.350	-0.360	53.95
6	1.251	1.254	0.28	-0.350	-0.357	25.75
7	1.251	1.252	0.07	-0.350	-0.325	16.20
8	1.251	1.251	0.03	-0.350	-0.449	11.01
9	1.251	1.272	1.65	-0.350	-0.318	82.97
10	1.251	1.258	0.59	-0.350	-0.343	40.11
11	1.251	1.253	0.19	-0.350	-0.348	25.83
12	1.251	1.252	0.05	-0.350	-0.372	18.24
13	1.251	1.278	2.18	-0.350	-0.234	112.36
14	1.251	1.262	0.91	-0.350	-0.304	54.59
15	1.251	1.256	0.38	-0.350	-0.163	35.58
16	1.251	1.254	0.22	-0.350	-0.310	25.50
17	1.251	1.285	2.76	-0.350	-0.162	141.73
18	1.251	1.265	1.13	-0.350	-0.171	69.19
19	1.251	1.258	0.53	-0.350	-0.240	45.23
20	1.251	1.254	0.24	-0.350	-0.218	32.78

In this study, it is set $N_s = N_{comb_s}$. In particular, to assess how the estimation accuracy is affected by the supposed coefficients, $\tilde{\beta}_0$ and $\tilde{\alpha}_{PM0}$, two different cases are analyzed: in the first one the coefficients are defined according to the criteria in Section III-C, i.e., $\tilde{\beta}_0 = 1.0 \cdot 10^{-6}$/Hz^2 and $\tilde{\alpha}_{PM0} = -0.1\%/°$C; in the second case the parameters are $\tilde{\beta}_0 = 1.5 \cdot 10^{-6}$/Hz^2 and $\tilde{\alpha}_{PM0} = -0.05\%/°$C.

In this study, two performance parameters are considered: the mean absolute percentage error (MAPE) and the number of accepted estimations, both averaged over the N_s trials. Fig. 5(a) reports the MAPE for the estimations of ψ_m and R. Note that, although case study is affected by high parameter variations, the estimation accuracy of ψ_m is very high in both cases. Also, the estimation accuracy of R is high even if it is significantly lower compared to the estimated ψ_m. This is mainly due to the fact that the stator resistance is more affected by the OCs variations (both temperature and frequency). Fig. 5(b) shows that most of the estimations of ψ_m have been accepted OCs while several estimations of R are rejected. In other words, not for every OC has been possible to match an auxiliary OC satisfying all the requirements in Algorithm 3. It is worth highlighting that, when only 2 OCs are available, an average of 0.67 and 0.32 estimations of ψ_m and R are accepted in the first case, while an average of 0.70 and 0.22 are accepted in the second case. This means that when only 2 OCs are available, the estimation of R is rejected more than 50% of the cases. Overall, the figure shows that the obtained results are not significantly affected by the values of the supposed coefficients.

Table IV reports the computational times required to perform 1000 estimations of ψ_m and R with $k_s = 1, 2, ..., 6$ using a MATLAB implementation of the proposed algorithm on pc equipped with an Intel Xeon CPU E5-1620 v2 @3.50GHz processor and a 16Gb RAM. The reported computational times include the time required to perform the initial estimations according to (32), (33), (35), and (36), the time required

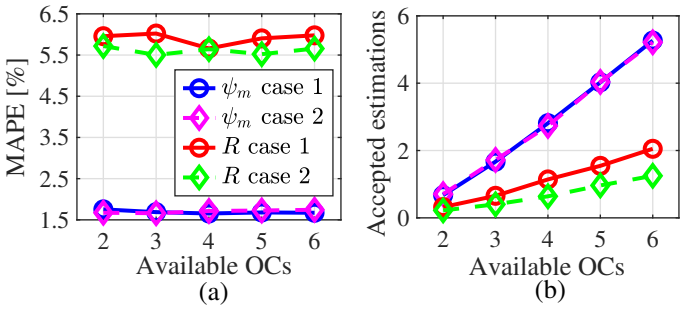

Fig. 5: Estimation of ψ_m and R in different scenarios: (a) MAPE of the estimation results, (b) average number of accepted estimations compared with the number of available OCs.

to select the AOCs according to Algorithm 3, and the time required by the coupled AdNNs to satisfy the stop condition (11). Note that, the time required for the estimation of R is slightly lower due to a higher rate of rejection of the estimations.

TABLE IV: Computational times

k_s	ψ_m	R
2	85 s	85 s
3	100 s	93 s
4	100 s	97 s
5	110 s	97 s
6	120 s	103 s

Instead, Table V and Table VI summarize the results obtained considering the full set of the OCs. The initial estimations needed to compute the majorants of the systematic errors obtained with procedure outlined in Section III-E are $\tilde{R}_0 = 0.56\Omega$ and $\hat{\psi}_0 = 28.08$ mWb. The tables list both the systematic errors and the error majorants computed using (24), (26) and (27), (28), respectively.

As first consideration, it is worth noticing that, for both resistance and rotor flux linkage, the systematic errors are very similar to the actual errors, except for small variations mainly due to measurement errors. This in an important achievement that proves the validity of the convergence and error analysis. The stator resistance has been estimated only for ten OCs while the rotor flux linkage estimations have been performed in all the available OCs. In addition, the estimation errors of the stator resistance are greater than the estimation errors of

TABLE V: Stator resistance estimation

MOC	AOC	R [Ω]	$\hat{R}$ [Ω]	Actual error [%]	Systematic error [%]	Error majorant [%]	Actual error n.c. [%]
1	13	0.7416	0.6428	-13.32	-12.28	21.43	-1.48
2	17	0.7771	0.7551	-2.84	-3.10	6.75	-4.91
3	15	0.8448	0.7681	-9.08	-9.39	11.89	18.00
4	16	0.9630	0.8888	-7.70	-8.48	9.65	18.01
5	2	0.7871	0.8022	1.92	1.18	16.06	-0.74
6	17	0.8254	0.7899	-4.30	-3.68	16.47	-26.56
9	2	0.8584	0.7807	-9.05	-9.63	21.36	-9.72
10	3	0.8996	0.8579	-4.63	-4.87	22.54	2.00
11	4	0.9748	1.008	3.42	2.61	21.17	13.27
13	4	0.9447	1.035	9.56	8.99	23.97	5.03

the rotor flux linkage. In fact, the mean absolute errors are 6.6% and 1.5%, respectively.

The rightmost column of Table V and Table VI report the estimation errors of both resistance and rotor flux linkage when the actuation delay is not compensated. Comparing these errors (with and without compensation) it can be inferred that the actuation delay compensation leads, on average, to a better estimation of both parameters.

V. Experimental Results

In this section, the proposed estimation procedure has been applied using the experimental data of a high speed PMSM whose main specifications are reported in Table I. A view of the main components of the instrumented test rig where the PMSM has been tested is reported in Fig. 6. The PMSM is loaded by another motor through a gearbox (ratio 1:5.975) and a torque meter. A custom designed SiC three-phase full-bridge converter has been adopted for the machine supply [29], while the control logic has been implemented on a Xilinx Zynq7020 SoC [30]. The measurements/data collected during the efficiency characterization of this machine (all listed in Table II) have been used to validate the proposed estimation method. In this case, each OC contains 10000 samples. Let's underline that the employed data have been obtained via experimental tests not aimed at the parameter estimation. Fig. 7 shows the main variables acquired during an operating condition at 30 krpm and rated current.

A. Inductance and distorted voltage term estimations

Fig. 8 shows the dynamic of the estimated q-axis inductance in OC 5 with $\lambda = 0.95$. The estimation rapidly converges to the measured value with a dynamic very similar to the simulation case. Table VII shows the results of the q-axis stator inductance and distorted voltage estimation. As in the simulation study, a good accuracy of the estimations of the q-axis inductance is achieved, with an average error of 0.93%.

TABLE VI: Rotor flux linkage estimation

MOC	AOC	ψ_m [mWb]	$\hat{\psi}_m$ [mWb]	Actual error [%]	Systematic error [%]	Error majorant [%]	Actual error n.c. [%]
1	13	26.74	26.35	-1.45	-0.94	1.38	0.14
2	17	26.62	26.35	-1.03	-0.50	0.92	0.10
3	15	26.40	25.62	-2.96	-2.51	2.72	6.55
4	16	26.00	24.90	-3.90	-3.50	3.50	9.83
5	2	26.72	26.61	-0.40	2.08	0.57	0.63
6	17	26.59	26.37	-0.86	-0.32	1.24	-0.06
7	18	26.37	26.14	-0.89	-0.34	3.40	4.53
8	19	25.98	25.90	-0.30	0.23	6.79	10.30
9	2	26.90	26.49	-0.75	0.93	0.55	0.60
10	3	26.57	26.37	-0.77	1.17	1.24	3.37
11	4	26.35	26.32	-0.11	0.27	1.94	7.03
12	4	25.97	25.08	-3.44	-3.08	3.73	7.98
13	4	26.69	26.62	-0.26	0.22	0.49	1.00
14	4	26.57	26.48	-0.35	0.16	1.12	4.37
15	4	26.36	26.07	-1.12	-0.70	1.98	7.67
16	4	25.99	24.99	-3.86	-3.45	3.38	9.87
17	4	26.66	26.49	-0.61	-0.09	0.52	0.46
18	4	26.54	26.28	-0.97	-0.46	1.17	4.35
19	4	26.33	25.79	-2.02	-1.55	2.03	8.14
20	4	25.94	24.72	-4.72	-4.31	3.71	11.13

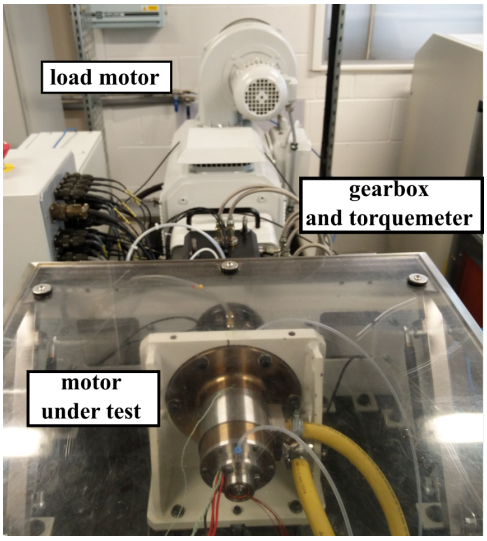

Fig. 6: Experimental setup layout.

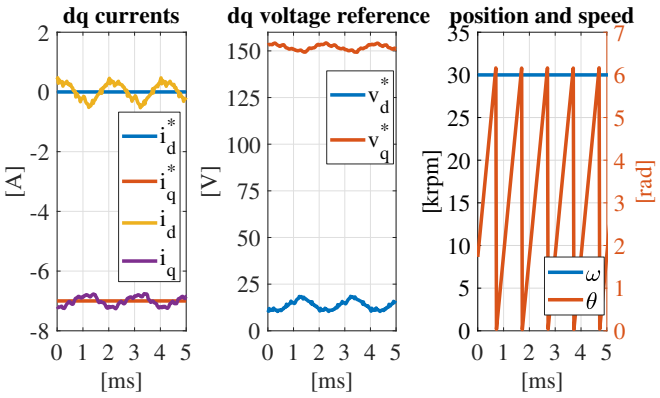

Fig. 7: Experimental data related to OC 18 used for the parameter estimation: dq currents, dq reference voltage, rotor position and speed.

For some OCs, the estimation errors may be slightly higher due to measurement errors or additional phenomena neglected in the PMSM model. Note that, even if the case study is not affected by inductance variations, the proposed algorithm can effectively track the inductance of motors affected by saturation effects since only an OCs is needed to estimate L_q. It can also be noted that the estimated distorted voltage generally increases in the OCs with high values of the q-axis current. This is justified by the increment of the voltage drops on the active switch and freewheeling diode with the temperature, which in turn depends on the amplitude of the currents.

B. Resistance and rotor flux linkage estimations

This subsection reports the experimental results on the estimation of R and ψ_m. To further assess the merits of the proposed method, a comparative analysis with other approaches from the literature is also presented. Since the proposed method has been designed to operate in scenarios where signal injections, dedicated tests and additional measurement

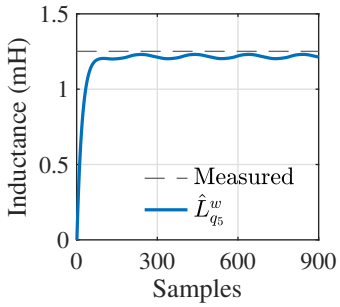

Fig. 8: Inductance estimation dynamic in OC 5.

TABLE VII: Stator inductance and distorted voltage term experimental estimations

OC	L_q [mH]	$\hat{L}_q$ [mH]	Actual error [%]	$\hat{V}_{dead}$ [V]
1	1.251	1.253	0.18	-0.119
2	1.251	1.235	-1.27	-0.409
3	1.251	1.268	1.34	-0.575
4	1.251	1.234	-1.35	-0.644
5	1.251	1.262	0.91	-0.054
6	1.251	1.224	-2.18	-0.263
7	1.251	1.234	-1.37	-0.640
8	1.251	1.257	0.45	-0.351
9	1.251	1.262	0.87	-0.304
10	1.251	1.232	-1.56	-0.461
11	1.251	1.264	1.02	-0.308
12	1.251	1.254	0.27	-0.283
13	1.251	1.236	-1.18	-0.194
14	1.251	1.239	-0.95	-0.196
15	1.251	1.250	-0.04	-0.451
16	1.251	1.256	0.42	-0.853
17	1.251	1.235	-1.3	-0.324
18	1.251	1.254	0.24	-0.234
19	1.251	1.242	-0.76	-0.583
20	1.251	1.239	-0.94	-1.006

devices are not allowed, two alternative solutions suitable in these scenarios are considered. The first one is based on a largely adopted strategy where a parameter is set to its nominal value or offline measure and the other one is estimated using just a single OC [5], [9], [12], [15]. This method will hereafter be referred to as the fixed parameter (FP) method. When R is fixed to its DC nominal value or offline measure R_0, the estimation of ψ_m in a generic OC α can be obtained by using ADNN1 while substituting $R_0(1+\alpha(\bar{\Theta}_i-20)$ in place of $\hat{R}^{*^{(j-1)}}$ in (9). It should be noted that the changing DC stator resistance value with temperature is considered in this manner. In the same way, when ψ_m is fixed to its nominal value ψ_{m0}, R is identified by means of AdNN2 while substituting $\hat{\psi}_m^{*^{(j)}}$ with ψ_{m0} in (10). Since the data from a single OC are needed to estimate the parameters, it is obvious that the accuracy of this method does not depend on the number of available OCs.

The other approach adopts a more detailed PMSM model which takes into account the dependency of the parameters on the OCs, as in [21] and [23]. In these works, the PMSM inductances are expressed by polynomial functions of the dq-axis currents by means of additional coefficients to be estimated. In particular, the least squares (LS) method is used to estimate the parameters exploiting simultaneously measurements collected during multiple steady-state operations. According to this approach, in the present study (29) and (30) are included into (2) to express the dependency of R and ψ_m on the OCs. Thus, the following model is obtained considering the measurements at the end of each OC:

$$\bar{u}'_{q_\alpha} = \bar{i}_{q_\alpha} R_\alpha(\bar{\Theta}_\alpha, \bar{\omega}_\alpha) + \bar{\omega}_\alpha \psi_{m0} + \bar{\omega}_\alpha(\bar{\Theta}_\alpha - 20)\alpha'_{PM0}, \quad (41)$$

with $\bar{u}'_{q_\alpha} = \bar{\bar{u}}_{q_\alpha} + \bar{D}_{q_\alpha}\hat{V}_{dead_\alpha}$, $\alpha'_{PM0} = \psi_{m0}\alpha_{PM0}$, and

$$R_\alpha(\bar{\Theta}_\alpha, \bar{\omega}_\alpha) = R_{DC_0}\left(1+\alpha_0(\bar{\Theta}_\alpha - 20)\right)\left(1+\beta_0\left(\frac{\bar{\omega}_\alpha}{2\pi}\right)^2\right).$$

This model can be rewritten in the following form:

$$\bar{u}'_{q_\alpha} = \bar{i}'_{q_\alpha} R_{DC_0} + \bar{i}'_{q_\alpha}\bar{\omega}_\alpha^{'2}\beta'_0 + \bar{\omega}_\alpha\psi_{m0} + \bar{\omega}_\alpha(\bar{\Theta}_\alpha - 20)\alpha'_{PM0}, \quad (42)$$

where $\bar{i}'_{q_\alpha} = (1+\alpha_0(\bar{\Theta}_\alpha - 20))\bar{i}_{q_\alpha}$, $\bar{\omega}'_\alpha = \bar{\omega}_\alpha/2\pi$ and $\beta'_0 = R_{DC_0}\beta_0$. This model has 4 unknown parameters to be estimated (R_{DC_0}, β'_0, ψ_{m0}, α'_{PM0}) and is linear on these parameters. Therefore the classic linear LS method can be adopted for the parameter identification as in [21] and [23]. Finally, the estimations of R and ψ_m can be obtained using (29) and (30) by substituting the results provided by the LS.

Fig. 9 shows the estimation dynamics of R and ψ_m related to OC 5 with OC 2 as AOC ($r = 0.25$). The estimations are compared with the measured rotor flux linkage and AC stator resistance. Note that the estimation accuracy is high in both cases.

Instead, Fig. 10 shows the results obtained with the proposed method considering two scenarios with 2 and 5 available OCs, respectively. In both cases, the available OCs are randomly chosen among the full dataset in Table II and a number of trials determined by using (40) is evaluated. Considering that only experimental evaluations of ψ_m and R at room temperature are available, to correctly assess the achieved estimations, this figure shows the results achieved considering only a portion of MOCs, i.e. the OCs at temperature lower than 50 °C (see Table II). In particular, a temperature correction of the measured AC resistance according to (38) is performed. Note that this temperature correction can be considered reliable only at low speed and temperature [31]. Therefore, for the estimation of the stator resistance, only OCs 1, 2, 5, 6 and 9 are analyzed.

The figure shows the average values of the estimations obtained in the two scenarios compared with the ones obtained with the FP method. The estimations of ψ_m obtained with the proposed method are very similar in the two cases and higly accurate. Instead, in most of the OCs, the accuracy of the FP method is lower since this approach does not account for the variation of the stator resistance with motor speed. The average estimations of R provided by the proposed method are also accurate and can strictly follow the resistance variations with motor speed. In this case, the estimations in the OC 1 are rejected and are not shown in the figure. Furthermore, it has to be highlighted that, in this case, the estimation accuracy slightly improves in the scenario with 5 OCs. This proves that the DMA is able to improve the estimation accuracy when more OCs are available by selecting AOCs that minimize the error majorants. Even in this case the accuracy of the FP method is lower since this approach does not consider the variation of the rotor flux linkage with the temperature.

Fig. 11 reports the average performances obtained with the proposed and the LS method on the reduced subset considered in the previous figure and in scenarios with different number of available OCs, as in Fig. 5. Note that the LS method fails when less than 5 OCs are available while the proposed method ensures good performances. The analysis shows that the LS method can overcome the proposed method only in scenarios with a large number of available OCs. This comparison demonstrates that the proposed method is more suitable in contexts where dedicated tests cannot be performed to collect data from different OCs of the motor.

Finally, Table VIII summarizes the results of the stator resistance and rotor flux linkage estimation considering the full set of the OCs. In this case, the obtained initial estimations needed for the calculation of the majorants of the systematic errors are $\hat{R}_0 = 0.40\Omega$ and $\hat{\psi}_0 = 28.38$mWb. As it can be seen, the stator resistance estimations have been rejected in 14 OCs while the rotor flux linkage estimation has been performed in all the available OCs. This difference between the output of the DMA in the simulation and experimental case is due to the different values of the initial estimations $(\hat{R}_0, \hat{\psi}_0)$, which affects the error majorants. Albeit the different initial estimations between the simulation and the experimental verification, for a given MOC the same AOC has been chosen by the DMA for the stator resistance estimations. Regarding the rotor flux linkage estimation, low values of the error majorants have been achieved. Moreover, the values of the estimations are similar to the measured value at 20°C provided in Table I thus confirming the effectiveness of the proposed method.

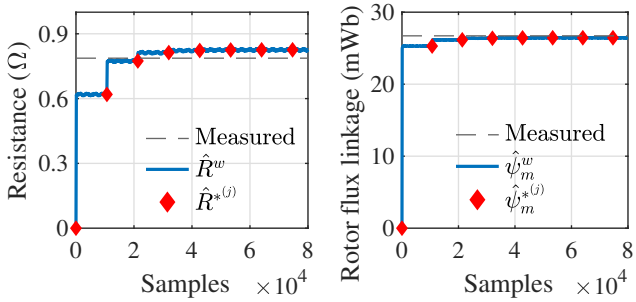

Fig. 9: Stator resistance and rotor flux linkage estimations dynamic related to OC 5.

VI. Conclusion

This work showed that it is possible to estimate the parameters of an isotropic permanent magnet synchronous machine exploiting regular measurements collected from in-service standard drives. Indeed, no additional sensor, signal injection, information on nominal values or dedicated test are required to carry out the estimations. The only requirement is the availability of measurements of multiple operating conditions. The lack of voltage measurements is treated by considering both inverter non-linearity and actuation delays. This feature allows the application of the proposed approach also at medium and high speed operation. An Adaline Neural Network (AdNN) estimates the q-axis inductance while the distorted voltage

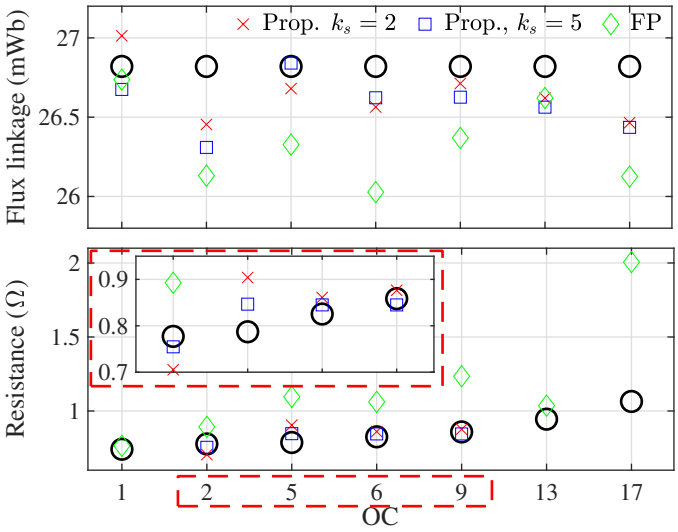

Fig. 10: Estimations of ψ_m and R with 2 and 5 OCs compared with the FP method. The black circles denote measured values.

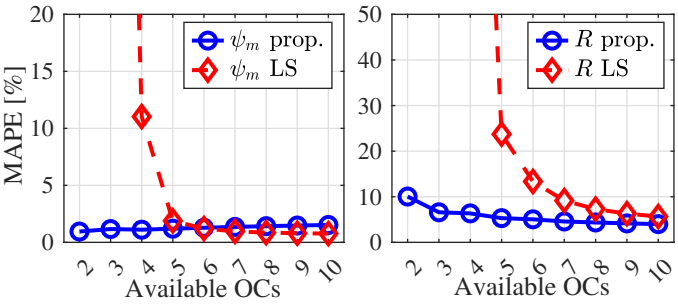

Fig. 11: Estimations of ψ_m and R in different scenarios with the proposed and the LS method.

TABLE VIII: Stator resistance and rotor flux linkage experimental estimations

MOC	AOC	$\hat{\psi}_m$ [mWb]	Error majorant [%]	AOC	$\hat{R}$ [Ω]	Error majorant [%]
1	13	26.57	1.21	n.a.	n.a.	n.a.
2	17	26.13	0.78	17	0.7678	8.12
3	15	25.59	2.09	15	0.7281	12.93
4	16	25.24	2.54	16	0.9430	9.89
5	2	26.44	0.51	2	0.8231	20.04
6	17	26.17	1.14	17	0.8270	21.26
7	18	26.01	3.19	n.a.	n.a.	n.a.
8	19	26.20	6.52	n.a.	n.a.	n.a.
9	2	26.44	0.44	2	0.8227	23.76
10	3	26.48	1.04	n.a.	n.a.	n.a.
11	4	26.30	1.76	n.a.	n.a.	n.a.
12	4	25.18	2.71	n.a.	n.a.	n.a.
13	2	26.71	0.43	n.a.	n.a.	n.a.
14	3	26.06	1.00	n.a.	n.a.	n.a.
15	4	26.23	1.68	n.a.	n.a.	n.a.
16	4	25.24	2.41	n.a.	n.a.	n.a.
17	2	26.13	0.41	n.a.	n.a.	n.a.
18	3	25.98	0.97	n.a.	n.a.	n.a.
19	4	26.05	1.64	n.a.	n.a.	n.a.
20	4	24.72	2.69	n.a.	n.a.	n.a.

term of the inverter is estimated via optimization. Then, the stator resistance and the rotor flux linkage are identified using two coupled AdNNs. The rank-deficiency issue is solved by using two different operating conditions. The criteria of

selecting the two operating conditions minimizing the estimation errors have been rigorously proved. Both simulation and experimental validations showed a high accuracy of the rotor flux linkage and q-axis inductance estimations with mean absolute errors lower than 2%. Satisfactory results have been also achieved in the identification of the stator resistance, which is the most difficult parameter to estimate due to its high dependency on the motor temperature and frequency. Finally, the comparison with alternative methods from the literature demonstrates the superiority of the proposed one in contexts where additional sensors, ad hoc tests and signal injections are impracticable.

VII. Acknowledgement

This work was supported in part by the Project Fondo di finanziamento della Ricerca di Sistema elettrico nazionale Piano Triennale 2019-2021 – Bando b – progetto "InSITE – INtelligent energy management of Smartgrids based on IoT and edge/cloud Technologies", riferimento Prog. CSEAB_00320; and in part by the Project Partenariato Esteso Network 4 Energy Sustainable Transition – NEST CUP D93C22000900001.

Appendix A
AdNN for parameter estimation

Fig. 12 shows a basic AdNN with one neuron, where I is the input, $\hat{O}$ and O are the estimated and measured output, W is the weight, and B is the bias. The estimated output is computed as follows:

$$\hat{O}(k) = I(k)W(k-1) + B(k). \tag{A.1}$$

At each step, the weight is updated to minimize the output error according to the following update law:

$$W(k) = W(k-1) - \eta I(k)(O(k) - \hat{O}(k)), \tag{A.2}$$

where η is the learning rate. By substituting (A.1) in (A.2), the following first-order difference equation is obtained:

$$W(k) = W(k-1)(1+\eta I^2(k)) - \eta I(k)(O(k) - B(k)), \tag{A.3}$$

whose solution is:

$$W(k) = c(-1-\eta I^2(k))^k + \frac{O(k)-B(k)}{I(k)}, \tag{A.4}$$

where c is real constant. The solution is asymptotically stable if η is chosen according to:

$$|-1-\eta I^2(k)| = \lambda, \quad \lambda < 1, \tag{A.5}$$

where λ is the chosen eigenvalue. Note that the solution convergence speed increases as λ approaches zero.

Appendix B
Influence of the measurement errors

This appendix reports the analysis of the influence of measurement errors on the parameter estimation accuracy considering compensated voltage errors (ε_{ud}, ε_{uq}), q-axis current error (ε_{iq}), rotor speed error (ε_{ω}), and rotor position offset error (ε_{θ}).

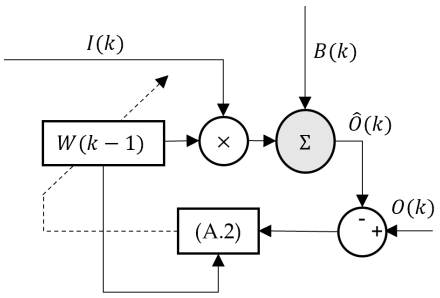

Fig. 12: AdNN.

The model of the PMSM accounting for ε_{ud}, ε_{uq}, ε_{iq}, and ε_{ω} can be expressed as follows:

$$\tilde{u}_d = -L_q(\omega+\varepsilon_\omega)(i_q+\varepsilon_{iq}) - D_d V_{dead} + \varepsilon_{ud}, \tag{B.1a}$$
$$\tilde{u}_q = R(i_q+\varepsilon_{iq}) + \psi_m(\omega+\varepsilon_\omega) - D_q V_{dead} + \varepsilon_{uq}. \tag{B.1b}$$

Let us consider (7). It can be shown that, if the learning rate is correctly chosen, the steady state value of $\hat{L}_{q_i}^w$ has the following expression:

$$\hat{L}_{q_i}^w(\infty) = -\frac{\bar{\tilde{u}}_i}{\bar{\omega}_i \bar{\tilde{i}}_{q_i}}, \tag{B.2}$$

where the generic variable $\bar{x}_i$ stands for $x_i\,(N_i)$. By substituting (B.1a) in (B.2), the steady-state estimation can be expressed as follows:

$$\hat{L}_{q_i}^w(\infty) = L_{q_i} + \frac{L_{q_i}\varepsilon_{iq}\varepsilon_\omega}{\bar{\omega}_i\bar{\tilde{i}}_{q_i}} + \frac{L_{q_i}\varepsilon_{iq}}{\bar{\tilde{i}}_{q_i}} + \frac{L_{q_i}\varepsilon_\omega}{\bar{\omega}} - \frac{\varepsilon_{ud}}{\bar{\omega}\bar{\tilde{i}}_{q_i}}, \tag{B.3}$$

in which the term related to $D_d V_{dead}$ has been neglected. Note that the estimation errors caused by measurement errors are reduced with the increase of both speed and current.

By substituting (B.1b) in (13) and by repeating the same procedure for the stator resistance, the followings are obtained:

$$\hat{\psi}_m^{*(j)} = \frac{R_\alpha(\bar{\tilde{i}}_{q_\alpha}+\varepsilon_{i_{q_\alpha}}) + \psi_{m_\alpha}(\bar{\omega}_\alpha+\varepsilon_{\omega_\alpha})}{\bar{\omega}_\alpha} + \frac{\varepsilon_{u_{q_\alpha}} - \hat{R}^{*(j-1)}\bar{\tilde{i}}_{q_\alpha}}{\bar{\omega}_\alpha}, \tag{B.4}$$

$$\hat{R}^{*(j-1)} = \frac{R_\beta(\bar{\tilde{i}}_{q_\beta}+\varepsilon_{i_{q_\beta}}) + \psi_{m_\beta}(\bar{\omega}_\beta+\varepsilon_{\omega_\beta})}{\bar{\tilde{i}}_{q_\beta}} + \frac{\varepsilon_{u_{q_\beta}} - \hat{\psi}^{*(j-1)}\bar{\omega}_\beta}{\bar{\tilde{i}}_{q_\beta}}. \tag{B.5}$$

By substituting (B.5) in (B.4), the following expression of the estimated rotor flux linkage is achieved:

$$\hat{\psi}_m^{*(\infty)} = \psi_{m_\alpha} + \varepsilon_{\psi_{m_\alpha}} + \varepsilon_{\psi_M}. \tag{B.6}$$

ε_{ψ_M} is the estimation error related to the measurement errors:

$$\varepsilon_{\psi_M} = \frac{\psi_{m_\alpha}\varepsilon_{\omega_\alpha} - \psi_{m_\beta}\varepsilon_{\omega_\beta}\bar{\tilde{i}}_{q_\alpha}/\bar{\tilde{i}}_{q_\beta}}{\bar{\omega}_\alpha(1-r)} + \frac{(R_\alpha\varepsilon_{i_{q_\alpha}} - R_\beta\varepsilon_{i_{q_\beta}}\bar{\tilde{i}}_{q_\alpha}/\bar{\tilde{i}}_{q_\beta}) + (\varepsilon_{u_{q_\alpha}} - \varepsilon_{u_{q_\beta}}\bar{\tilde{i}}_{q_\alpha}/\bar{\tilde{i}}_{q_\beta})}{\bar{\omega}_\alpha(1-r)}. \tag{B.7}$$

By repeating the same procedure for the stator resistance, the following expression is achieved:

$$\hat{R}^{*(\infty)} = R_\alpha + \varepsilon_{R_\alpha} + \varepsilon_{R_M}. \tag{B.8}$$

ε_{R_M} is the estimation error related to the measurement errors:

$$\varepsilon_{R_M} = \frac{\psi_{m_\beta}\varepsilon_{\omega_\beta} - \psi_{m_\alpha}\varepsilon_{\omega_\alpha}\bar{\omega}_\beta/\bar{\omega}_\alpha}{\bar{i}_{q_\beta}(1-r)} + \\ + \frac{(R_\beta\varepsilon_{i_{q_\beta}} - R_\alpha\varepsilon_{i_{q_\alpha}}\bar{\omega}_\beta/\bar{\omega}_\alpha) + (\varepsilon_{u_{q_\beta}} - \varepsilon_{u_{q_\alpha}}\bar{\omega}_\beta/\bar{\omega}_\alpha)}{\bar{i}_{q_\beta}(1-r)}. \tag{B.9}$$

Analysing (B.7) and (B.9), it can be inferred that the value of r has a great influence on the amplification of the estimation errors related to the measurement. Therefore, it is recommended to avoid estimations with $0.5 < r < 1$.

The PMSM model accounting for ε_θ is the following [17]:

$$\tilde{u}_d = -L_q\omega i_q - \psi_m\omega\sin(\varepsilon_\theta) - D_dV_{dead}, \tag{B.10a}$$
$$\tilde{u}_q = Ri_q + \psi_m\omega\cos(\varepsilon_\theta) - D_qV_{dead}. \tag{B.10b}$$

By substituting (B.10a) in (B.2) and by neglecting the term D_dV_{dead}, the steady-state q-axis inductance estimation can be expressed as follows:

$$\hat{L}^w_{q_i}(\infty) = L_{q_i} + \varepsilon_{L_\theta} = L_{q_i} + \frac{\psi_{m_i}\sin(\varepsilon_\theta)}{\bar{i}_{qi}}. \tag{B.11}$$

As it can be seen, the estimation error ε_{L_θ} increases as ε_θ increases, while decreases as the i_q and the temperature increase. In fact, ψ_m decreases with the increase of the temperature.

By substituting (B.10b) in (13) and by repeating the same procedure for the stator resistance, the followings are obtained:

$$\hat{\psi}^{*(j)}_m = \frac{R_\alpha\bar{i}_{q_\alpha} + \psi_{m_\alpha}\bar{\omega}_\alpha\cos(\varepsilon_\theta) - \hat{R}^{*(j-1)}\bar{i}_{q_\alpha}}{\bar{\omega}_\alpha}, \tag{B.12}$$

$$\hat{R}^{*(j-1)} = \frac{R_\beta\bar{i}_{q_\beta} + \psi_{m_\beta}\bar{\omega}_\beta\cos(\varepsilon_\theta) - \hat{\psi}^{*(j-1)}_m\bar{\omega}_\beta}{\bar{i}_{q_\beta}}. \tag{B.13}$$

By substituting (B.13) in (B.12), if $r < 1$, the following steady-state expression of the estimated rotor flux linkage is achieved:

$$\hat{\psi}^{*(\infty)}_m = \psi_{m_\alpha} + \varepsilon^{'}_{\psi_{m_\alpha}} + \varepsilon_{\psi_\theta}, \tag{B.14}$$

where

$$\varepsilon^{'}_{\psi_{m_\alpha}} = \frac{(\psi_{m_\alpha} - \psi_{m_\beta})r}{1-r}\cos(\varepsilon_\theta) + \frac{(R_\alpha - R_\beta)\frac{\bar{i}_{q_\beta}}{\bar{\omega}_\alpha}}{1-r}, \tag{B.15}$$

$$\varepsilon_{\psi_\theta} = -\psi_{m_\alpha}(1-\cos(\varepsilon_\theta)). \tag{B.16}$$

Note that the first component of $\varepsilon^{'}_{\psi_{m_\alpha}}$ is favorably affected by ε_θ while $\varepsilon_{\psi_\theta}$ increases with the increase of ε_θ. It is worth underlying that $\varepsilon_{\psi_\theta}$ cannot be mitigated by a proper selection of the OCs. Therefore, the consideration of the offset position error for the computation of the majorants of the systematic error does not affect the selection of the AOCs by the DMA.

With the same procedure, the estimated stator resistance has the following expression;

$$\hat{R}^{*(\infty)} = R_\alpha + \varepsilon^{'}_{R_\alpha}. \tag{B.17}$$

where

$$\varepsilon^{'}_{R_\alpha} = \frac{R_\beta - R_\alpha}{1-r} + \frac{(\psi_{m_\beta} - \psi_{m_\alpha})\frac{\bar{\omega}_\beta}{\bar{i}_{q_\beta}}}{1-r}\cos(\varepsilon_\theta). \tag{B.18}$$

Even in this case, the second component of $\varepsilon^{'}_{R_\alpha}$ is favorably affected by ε_θ but there is no error component equivalent to $\varepsilon_{\psi_\theta}$.

REFERENCES

[1] Z. Li, G. Feng, C. Lai, D. Banerjee, W. Li, and N. C. Kar, "Current injection-based multi-parameter estimation for dual three-phase ipmsm considering vsi nonlinearity," *IEEE Trans. Transport. Electrif.*, vol. 5, no. 2, pp. 405–415, 2019.

[2] K. Liu, Q. Zhang, J. Chen, Z. Q. Zhu, and J. Zhang, "Online multiparameter estimation of nonsalient-pole pm synchronous machines with temperature variation tracking," *IEEE Trans. Ind. Electron.*, vol. 58, no. 5, pp. 1776–1788, 2011.

[3] K. Liu and Z. Q. Zhu, "Position-offset-based parameter estimation using the adaline nn for condition monitoring of permanent-magnet synchronous machines," *IEEE Trans. Ind. Electron.*, vol. 62, no. 4, pp. 2372–2383, 2015.

[4] M. S. Rafaq and J.-W. Jung, "A comprehensive review of state-of-the-art parameter estimation techniques for permanent magnet synchronous motors in wide speed range," *IEEE Trans. Ind. Informat.*, vol. 16, no. 7, pp. 4747–4758, 2020.

[5] Z. Q. Zhu, D. Liang, and K. Liu, "Online parameter estimation for permanent magnet synchronous machines: An overview," *IEEE Access*, vol. 9, pp. 59 059–59 084, 2021.

[6] O. Sandre-Hernandez, R. Morales-Caporal, J. Rangel-Magdaleno, H. Peregrina-Barreto, and J. N. Hernandez-Perez, "Parameter identification of pmsms using experimental measurements and a pso algorithm," *IEEE Trans. Instrume. Meas.*, vol. 64, no. 8, pp. 2146–2154, 2015.

[7] C. Candelo-Zuluaga, J.-R. Riba, and A. Garcia, "Pmsm parameter estimation for sensorless foc based on differential power factor," *IEEE Trans. Instrum. Meas.*, vol. 70, pp. 1–12, 2021.

[8] G. Feng, C. Lai, K. Mukherjee, and N. C. Kar, "Current injection-based online parameter and vsi nonlinearity estimation for pmsm drives using current and voltage dc components," *IEEE Trans. Transport. Electrif.*, vol. 2, no. 2, pp. 119–128, 2016.

[9] T. Boileau, N. Leboeuf, B. Nahid-Mobarakeh, and F. Meibody-Tabar, "Online identification of pmsm parameters: Parameter identifiability and estimator comparative study," *IEEE Trans. on Ind. Appl.*, vol. 47, no. 4, pp. 1944–1957, 2011.

[10] Y. Shi, K. Sun, L. Huang, and Y. Li, "Online identification of permanent magnet flux based on extended kalman filter for ipmsm drive with position sensorless control," *IEEE Trans. Ind. Electron.*, vol. 59, no. 11, pp. 4169–4178, 2012.

[11] C. Lian, F. Xiao, J. Liu, and S. Gao, "Parameter and vsi nonlinearity hybrid estimation for pmsm drives based on recursive least square," *IEEE Trans. Transp. Electrification*, pp. 1–1, 2022.

[12] M. A. Hamida, J. De Leon, A. Glumineau, and R. Boisliveau, "An adaptive interconnected observer for sensorless control of pm synchronous motors with online parameter identification," *IEEE Trans. Ind. Electron.*, vol. 60, no. 2, pp. 739–748, 2013.

[13] F. K. Ramdane Tami, Driss Boutat and R. E. Gouri, "Rotor speed, load torque and parameters estimations of a permanent magnet synchronous motor using extended observer forms," *IET Control Theory & Applications*, vol. 11, pp. 1485–1492, 2017.

[14] O. C. Kivanc and S. B. Ozturk, "Sensorless pmsm drive based on stator feedforward voltage estimation improved with mras multiparameter estimation," *IEEE/ASME Trans. Mechatronics*, vol. 23, no. 3, pp. 1326–1337, 2018.

[15] X. Li and R. Kennel, "General formulation of kalman-filter-based online parameter identification methods for vsi-fed pmsm," *IEEE Trans. Ind. Electron.*, vol. 68, no. 4, pp. 2856–2864, 2021.

[16] Z. Liu, X. Fan, W. Kong, L. Cao, and R. Qu, "Improved small-signal injection-based online multiparameter identification method for ipm machines considering cross-coupling magnetic saturation," *IEEE Trans. Power Electron.*, vol. 37, no. 12, pp. 14 362–14 374, 2022.

[17] K. Liu and Z. Q. Zhu, "Position offset-based parameter estimation for permanent magnet synchronous machines under variable speed control," *IEEE Trans. Power Electron.*, vol. 30, no. 6, pp. 3438–3446, 2015.

[18] X. Xiao, C. Chen, and M. Zhang, "Dynamic permanent magnet flux estimation of permanent magnet synchronous machines," *IEEE Trans. Appl. Supercond.*, vol. 20, no. 3, pp. 1085–1088, 2010.

[19] B. Stumberger, B. Kreca, and B. Hribernik, "Determination of parameters of synchronous motor with permanent magnets from measurement of load conditions," *IEEE Trans. Energy Convers.*, vol. 14, no. 4, pp. 1413–1416, 1999.

[20] E. Armando, R. I. Bojoi, P. Guglielmi, G. Pellegrino, and M. Pastorelli, "Experimental identification of the magnetic model of synchronous machines," *IEEE Trans. Ind. Appl.*, vol. 49, no. 5, pp. 2116–2125, 2013.

[21] C. Lai, G. Feng, Z. Li, and N. C. Kar, "Computation-efficient decoupled multiparameter estimation of pmsms from massive redundant measurements," *IEEE Trans. Power Electron.*, vol. 35, no. 10, pp. 10 729–10 740, 2020.

[22] K. Liu, Z. Q. Zhu, Q. Zhang, and J. Zhang, "Influence of nonideal voltage measurement on parameter estimation in permanent-magnet synchronous machines," *IEEE Trans. Ind. Electron.*, vol. 59, no. 6, pp. 2438–2447, 2012.

[23] G. Feng, C. Lai, X. Tan, W. Peng, and N. C. Kar, "Multi-parameter estimation of pmsm using differential model with core loss compensation," *IEEE Trans. Transp. Electrification*, vol. 8, no. 1, pp. 1105–1115, 2022.

[24] E. Brescia, D. Costantino, F. Marzo, P. R. Massenio, G. L. Cascella, and D. Naso, "Automated multistep parameter identification of spmsms in large-scale applications using cloud computing resources," *Sensors*, vol. 21, no. 14, p. 4699, Jul. 2021.

[25] B.-H. Bae and S.-K. Sul, "A compensation method for time delay of full-digital synchronous frame current regulator of pwm ac drives," *IEEE Trans. Ind. Appl.*, vol. 39, no. 3, pp. 802–810, 2003.

[26] R. R. Rhinehart, "Automated steady and transient state identification in noisy processes," in *2013 American Control Conference*, pp. 4477–4493, 2013.

[27] D. Fernandez, D. Hyun, Y. Park, D. Reigosa, S. B. Lee, D. M. Lee, and F. Briz, "Permanent magnet temperature estimation in pm synchronous motors using low cost hall effect sensors," in *2016 IEEE Energy Conversion Congress and Exposition (ECCE)*, pp. 1–8, 2016.

[28] S. Xiao and A. Griffo, "Online thermal parameter identification for permanent magnet synchronous machines," *IET Electric Power Applications*, vol. 14, no. 12, pp. 2340–2347, 2020.

[29] G. L. Calzo, P. Zanchetta, C. Gerada, A. Gaeta, and F. Crescimbini, "Converter topologies comparison for more electric aircrafts high speed starter/generator application," in *2015 IEEE Energy Conversion Congress and Exposition (ECCE)*, pp. 3659–3666, Sep. 2015.

[30] A. Galassini, G. Lo Calzo, A. Formentini, C. Gerada, P. Zanchetta, and A. Costabeber, "ucube: Control platform for power electronics," in *2017 IEEE Workshop on Electrical Machines Design, Control and Diagnosis (WEMDCD)*, pp. 216–221, 2017.

[31] R. Wrobel, D. E. Salt, A. Griffo, N. Simpson, and P. H. Mellor, "Derivation and scaling of ac copper loss in thermal modeling of electrical machines," *IEEE Trans. Ind. Electron.*, vol. 61, no. 8, pp. 4412–4420, 2014.

Elia Brescia received the M.Sc (Hons.) and Ph.D degrees in electrical engineering from Polytechnic University of Bari, Italy, in 2018, and 2022, respectively, where he is currently a research fellow. He is involved in several R&D projects and scientific consultancy activities with industrial partners in the fields of artificial intelligence and electrical machines and drives. His research interests include the design and control of permanent magnet synchronous machines and cloud-oriented approaches for the parameter identification of electrical machines in large-scale applications.

figure/Massenio.jpg

Paolo Roberto Massenio received the M.Sc (Hons.) and Ph.D degrees in control engineering from Polytechnic University of Bari, Italy, in 2017, and 2021, respectively. In 2019 and 2020, he was a Visiting Scholar with the University of Texas at Arlington, Arlington, TX. In 2021 he received a best paper award from the IEEE Power Electronic Society. He is currently a research fellow within Polytechnic University of Bari. His research interests include distributed control of microgrids, reinforcement learning for optimal control, novel control approaches for soft-robots, and system identification.

Mauro Di Nardo (M'18) received the M.Sc. (Hons.) degree in electrical engineering from the Polytechnic University of Bari, Italy, in 2012, and the Ph.D. degree in electrical machine design from the University of Nottingham, U.K., in 2017. From 2017 to 2019, he was Head with the AROL R&D Team within the Polytechnic University of Bari leading industrial projects on electrical drives design for mechatronics applications. Since the 2019, he is with the Power Electronics and Machine Control Group of the University of Nottingham as Research Fellow working on wide variety of projects. His research interests include the analysis, modelling, design optimizations and experimental characterization of permanent magnet and synchronous reluctance machines for automotive, aerospace and household sectors, induction motor for industrial applications as well as niche machine topologies such as bearingless and hysteresis motor. He serves as an Associate Editor for the Open Journal of Industry Applications.

Giuseppe Leonardo Cascella received his MSc degree with honors (2001) and his PhD in Electrical Engineering (2005) from the Polytechnic University of Bari (Italy), where is currently assistant researcher of the CEMD Research Group. He won two EU Marie Curie Fellowships at Nottingham University (UK) and the University of Malta. He completed his Postdoctoral Research project (2008) "Adaptive Memetic Algorithms for Electric Drives". He is the founder (2015) and CEO of Idea75.it. He published 70+ peer-reviewed scientific papers on industry 4.0 and AI applications, has been the coordinator of 30+ R&D industrial projects and received the following awards: 2018 AWS Activate Builder, "Cloud Data Analytics for Energy Efficiency", Amazon Web Services, 2018; best experiment in Open Call 2, BEinCPPS, H2020, EU funded, project 680633, 2018; "SmartSupervisor for Cognitive Energy Efficiency", A&T award for the best innovative i4.0 solution, 2017. He is a member of IEEE (Institute of Electrical and Electronics Engineers) and of the Italian National Order of Engineers.

Chris Gerada (SM'12) received the Ph.D. degree in the numerical modeling of electrical machines from the University of Nottingham, Nottingham, U.K., in 2005. He is currently an Associate Pro-Vice-Chancellor for Industrial Strategy and Impact, and a Professor of Electrical Machines. His current research interests include electromagnetic energy conversion in electrical machines and drives, focusing mainly on transport electrification. He has secured more than 20M of funding through major industrial, European and U.K. grants and authored more than 350 referred publications. He was a Researcher with the University of Nottingham on high-performance electrical drives and on the design and modeling of electromagnetic actuators for aerospace applications. In 2008, he was a Lecturer in electrical machines; in 2011, as an Associate Professor; and in 2013, as a Professor with the University of Nottingham.,Dr. Gerada was the recipient of the Research Chair from the Royal Academy of Engineering in 2013. He was an Associate Editor for IEEE Transactions on Industry Applications and is the past Chair of IEEE IES Electrical Machines Committee

Francesco Cupertino (SM'12) received the Laurea and Ph.D. degrees in electrical engineering from the Politecnico di Bari, Italy, in 1997 and 2001, respectively. Since 2001, he has been with the Department of Electrical and Information Engineering, Politecnico di Bari, Bari, Italy, where he is currently a Full Professor of converters, electrical machines, and drives. He is the Scientific Director of four public/private laboratories at Politecnico di Bari that enroll more than 50 researchers; the laboratory Energy Factory Bari, with GE AVIO, aimed at developing research projects in the fields of aerospace and energy; the More Electric Transportation laboratory, with CVIT SpA (BOSCH Group), aimed at developing technologies for sustainable mobility; Cyber Physical Systems AROL Bari, with AROL SpA, focused on closure systems for food and beverage; Innovation for Mills, with Casillo Group and Idea75, focused in the Industry4.0 applications for wheat processing. He has authored or coauthored more than 130 scientific papers on these topics. His research interests include the design of synchronous electrical machines, motion control of high performances electrical machines, applications of computational intelligence to control, and sensorless control of ac electric drives. He is currently the rector of Politecnico di Bari.